Mastella, G., Corbi, F., Funiciello, F., Rosenau, M. (2022): Foamquake: a novel analog model mimicking megathrust seismic cycles. - Journal of Geophysical Research: Solid Earth, 127, 3, e2021JB022789.

https://doi.org/10.1029/2021JB022789

ADVANCING EARTH AND SPACE SCIENCE

JGR Solid Earth

RESEARCH ARTICLE

10.1029/2021JB022789

Foamquake: A Novel Analog Model Mimicking Megathrust Seismic Cycles

G. Mastella[1], F. Corbi[2], F. Funiciello[1], and M. Rosenau[3]

[1]Dip Scienze, Laboratory of Experimental Tectonics, Università "Roma TRE", Rome, Italy, [2]Istituto di Geologia Ambientale e Geoingegneria – CNR c/o Dipartimento di Scienze della Terra, Sapienza Università di Roma, Rome, Italy, [3]Helmholtz Centre Potsdam, GFZ German Research Centre for Geosciences, Potsdam, Germany

Key Points:

- A novel seismotectonic model that reproduces realistically several characteristics of great subduction megathrust earthquakes is presented
- Analog earthquakes follow similar source parameters scaling as natural interplate earthquakes
- Along trench segmentation introduces complexity in space-time-rupture history, highlighting the importance of the 3D nature of the setup

Supporting Information:

Supporting Information may be found in the online version of this article.

Correspondence to:

G. Mastella,
giacomo.mastella@uniroma3.it

Citation:

Mastella, G., Corbi, F., Funiciello, F., & Rosenau, M. (2022). *Foamquake*: A novel analog model mimicking megathrust seismic cycles. *Journal of Geophysical Research: Solid Earth*, *127*, e2021JB022789. https://doi.org/10.1029/2021JB022789

Received 16 JUL 2021
Accepted 5 FEB 2022

Author Contributions:

Conceptualization: F. Corbi, F. Funiciello
Data curation: G. Mastella, F. Corbi, M. Rosenau
Formal analysis: G. Mastella, F. Corbi, M. Rosenau
Funding acquisition: F. Funiciello
Methodology: G. Mastella, F. Corbi, M. Rosenau
Project Administration: F. Funiciello
Software: G. Mastella, F. Corbi
Supervision: F. Corbi, F. Funiciello
Validation: G. Mastella, F. Corbi, F. Funiciello, M. Rosenau
Visualization: G. Mastella, F. Corbi, M. Rosenau
Writing – original draft: G. Mastella, F. Corbi, F. Funiciello
Writing – review & editing: G. Mastella, F. Corbi, F. Funiciello, M. Rosenau

Abstract

In the last decades, seismotectonic analog models have been developed to better understand many aspects of the seismic cycle. Differently from other lab-quake experiments, seismotectonic models mimic the first order characteristics of the seismic cycle in a scaled fashion. Here we introduce *Foamquake*: A novel seismotectonic model with a granular frictional interface that as a whole behaves elastoplastically. The model experiences cycles of elastic loading and release via spontaneous nucleation of frictional instabilities at the base of an elastic foam wedge, hereafter called foamquakes. These analog earthquakes show source parameters (i.e., moment-duration and moment-rupture area) scaling as great interplate earthquakes and a coseismic displacement of few tens of meters when scaled to nature. Models with two asperities separated by a barrier can be performed with *Foamquake* given the 3D nature of the setup. Such model configuration generates sequences of full and partial ruptures with different recurrence intervals as well as rupture cascades. By tuning the normal load acting on individual asperities, *Foamquake* reproduces superimposed cycles rupture patterns such as those observed along natural megathrusts. The physical properties of asperities and barriers affect model seismic behavior. Asperities with similar properties and low yield strength fail preferentially in a simultaneous manner. The combination of all those characteristics suggests that *Foamquake* is a valuable tool for investigating megathrust seismicity and seismic processes that depend on the 3D nature of the subduction environment.

Plain Language Summary

Despite earthquakes rank within the main geohazards, there are still several important open questions about their nature that remain unanswered or require additional investigation. Complementary to observational studies, a strategy often used by scientists to tackle this problem is to safely reproduce earthquakes with computer simulations or with laboratory experiments. Here we introduce a novel experimental model (*Foamquake*) that reproduces the largest earthquakes on Earth, those that occur at convergent plate boundaries like the Tohoku-oki earthquake that hit the Japanese Pacific coast in 2011. Our model has the distinctive characteristic of reproducing earthquakes in a scaled fashion; that is, lengths, velocities and forces are smaller but scaled with respect to real ones. Moreover, time is accelerated with regard to nature so that we do not wait hundreds of years to observe a lab-quake. Indeed, we are able to study the details of hundreds of them in a few minutes long experimental run. We report the details of the experimental model and focus on the arguments bringing us to consider our lab-quakes similar to real earthquakes. We demonstrate that the experimental setup can afford new insights for understanding the seismic behavior at convergent plate boundaries.

1. Introduction

The Earth's greatest earthquakes (e.g., the M_w9.1 2011 Tohoku earthquake) occur at the frictional interface between subducting oceanic- and overriding plates (i.e., the megathrust) at convergent margins (e.g., Pacheco & Sykes, 1992; Scholz, 1990). These events are the most devastating expression of Earth's dynamics and, together with tsunamis, they represent a major hazard to society. Unfortunately, due to the short period of instrumental records, the limited resolution/completeness of paleo-seismic archives, and the paucity of direct observations, many aspects of the megathrust seismic cycle remain poorly understood.

Numerical and analog modeling offers opportunities to investigate the controlling factors of subduction seismicity (e.g., Brizzi et al., 2020; Corbi, Herrendörfer et al., 2017; Sobolev & Muldashev, 2017). Both analog- and numerical models have pros and cons, hence researchers try to get the best from those models with combined studies (e.g., Corbi, Herrendörfer et al., 2017; van Dinther et al., 2013). Analog models are intrinsically 3D even if quasi-2D cylindrical setups have been often developed for simplicity (e.g., Corbi et al., 2013; Dominguez et al., 2015; Rosenau, Lohrmann & Oncken, 2009). Their setups can be easily tuned to perform parametric studies. Also numerical models can simulate seismic cycles in 3D but well-resolved parametric studies are still not affordable computationally.

Seismotectonic analog models are simplified reproductions of geodynamical systems at convenient spatial and temporal scales. Seismotectonic models feature both long-term, steady stress accumulation and rapid stress drops characteristics of seismic cycles. From the '70s to 90s foam rubber has been extensively used in seismotectonic modeling, because of easiness of handling this material for experimental setups (e.g., Archuleta & Brune, 1975; Brune, 1973; Brune et al., 1990). Foam models have shed light on the basic physics governing the sliding of frictional interfaces (Anooshehpoor & Brune, 1999; Brune, 1996; Brune & Anooshehpoor, 1997; Brune et al., 1993). However, several concerns affect foam rubber properties, including unavoidable edge effects related to its low rigidity, leading to a non-uniform stress distribution along the fault interface (Scholz et al., 1972), material nonlinearities and high friction coefficient (i.e., from 1 to 10, Anooshehpoor & Brune, 1994; Caniven et al., 2015), making the material inappropriate to reproduce the frictional behavior of natural faults (Rosakis et al., 2007). Hence, for several years, foam models have been abandoned. Caniven et al. (2015) coated the foam rubber with epoxy resin to decrease the frictional coefficient, opening new avenues for the use of foam rubber in seismotectonic modeling. Dominguez et al. (2015) and Caniven and Dominguez (2021) developed a quasi-2D subduction setup, using multi-layered visco-elastoplastic rheology capable of reproducing the whole seismic cycle, including viscoelastic post-seismic deformation.

However, these 2D models cannot adequately reproduce processes linked to the three-dimensional nature of megathrust shear zones and are affected by limitations about analog earthquakes scaling with respect to natural prototypes. Similar concerns regard other megathrust analog models, such as gelatine models of Corbi et al. (2013); Corbi, Funiciello et al. (2017), which generate analog earthquakes with an exaggerated amount of coseismic slip when scaled to natural interplate earthquakes. Models using bulk mixtures of granular materials (e.g., rubber pellets, rice, and sugar) experience properly scaled ruptures in 2D (Rosenau et al., 2010), but may overestimate peak slip and strain in 3D (Rosenau et al., 2019)]. In addition, all of these setups dimensions scale with a maximum of ~240 km along trench, allowing to keep partly into account the importance of the along trench earthquake growth. Larger setups scaling is required to reproduce earthquakes like the 2011 Tohoku or the 2010 Maule (e.g., Tsuda et al., 2017; Yue et al., 2014) as well as complex space-time ruptures patterns observed at subduction zones. These patterns include the existence of "permeable" (to rupture propagation) barriers, quasi-periodic recurrence behavior, rupture cascades, and superimposed cycles (Philibosian & Meltzner, 2020), features strongly linked to the 3D interacting nature of the system.

Here we introduce a novel 3D seismotectonic analog model baptized *Foamquake*, referring to the material of the model wedge. The model reproduces a 510 km long (in trench parallel direction) subduction segment. The details of the experimental setup, modeling procedure, analysis and results are presented thoroughly in this article. *Foamquake* seismic behavior is compared with observations from real subduction zones, describing similarities in terms of source scaling and periodicity. Models with two neighboring asperities with equal and dissimilar properties are also presented, showing that this configuration reproduces space-time rupture histories as in the natural prototype.

2. Experimental Approach

2.1. Experimental Setup

The set-up is composed of a Plexiglass box where an elastic foam wedge with a dimension of $145 \times 90 \times 20$ cm^3 (i.e., the overriding plate) overlies a planar, 10° dipping, rigid plate (i.e., the subducting plate; Figure 1). Along the plate, a basal conveyer belt is driven with constant velocity (0.01 cm/s), reproducing a steady, trench-orthogonal subduction. A 1 cm thick layer of granular materials simulates the shear zone along the plate interface (i.e., the megathrust) and transfers frictional shear stress between the foam wedge and the conveyor belt (Figure 1c). The plate interface features a rectangular "seismogenic patch" made of rice (analog of a seismic asperity) surrounded by quartz sand. In the area of the asperity, we glued on the foam wedge base and on the conveyor belt 2 cm spaced stripes of rice grains trench-parallel aligned, to ensure coupling between the layers that is, wedge-asperity and subducting plate-asperity. The different materials in the granular layer are not confined laterally but accumulated shear is small enough to prevent mixing or geometric changes. The downdip width W of the seismogenic patch is 30 cm and its updip limit is 10 m from the trench.

The model is not affected by lateral friction acting at the two sides of the foam wedge which are free to move laterally and expand for up to 5 cm within the Plexiglass box. The wedge rear is confined by a rigid vertical backstop.

10.1029/2021JB022789

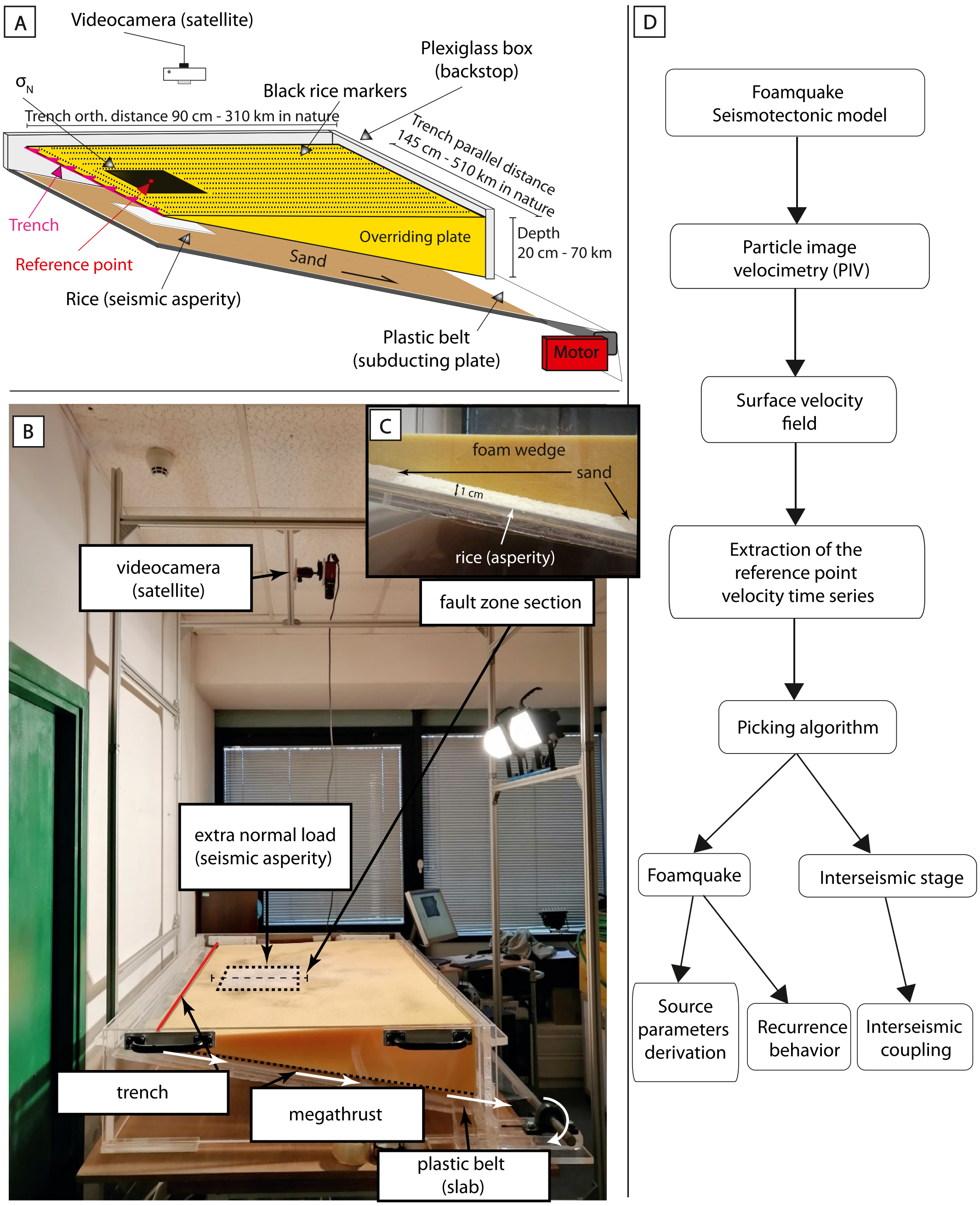

Figure 1. (a), (b) and (c) Experimental setup. A foam wedge (the upper lithospheric plate analog) overlays a planar, 10° inclined rigid plate (the subducting plate analog). The interface between the foam and plate mimics the megathrust interface. A plastic conveyor belt laying on the rigid plate moves downward at the constant velocity of 0.01 cm/s providing a continuous shear to the wedge base. Along the plate interface a seismic asperity made of rice is surrounded by sand reproducing the fault zone (c). At the model surface, a normal load is applied above the asperity. The model is monitored with a top-view high resolution camera (space-satellite analog). (d) Flow chart describing technical steps to derive coseismic and interseismic parameters from particle-image-velocimetry-derived velocity time series.

2.2. Rheological and Frictional Properties of Analog Materials

We used foam rubber (i.e., Resingomm SM_2) to simulate the elastic behavior of the lithosphere. Foam rubber is characterized by a Young modulus $E = 30$ kPa and a Poisson ratio $\nu = 0.1$ (Table S1 and Figure S1 in Supporting Information S1). Due to the low stress applied, the foam wedge is subject to particularly low strains ($\varepsilon < 0.02$), excluding possible nonlinearities in its deformation (Smardzewski et al., 2008).

The analog fault zone is a generic model of natural subduction shear zones. The analog megathrust configuration mimics the along dip heterogeneous frictional zonation observed at natural megathrusts (e.g., Lay et al., 1982), where the seismogenic zone is confined at its updip and downdip limits by aseismic zones (e.g., Hyndman et al., 1997). In our models, the updip and downdip limits of the analog seismogenic zone have been scaled with respect to the average value observed in nature (Section 2.3). *Foamquake* experiences emergent stick-slip behavior due the physical properties of granular materials placed along the megathrust resulting in the spontaneous nucleation of slip instabilities within the rice layer. The frictional strength of rice decreases with increasing shear rate similar to natural rocks causing stick-slip instability to emerge spontaneously (Rosenau, Lohrmann & Oncken, 2009). Accordingly, the rice patch represents a velocity weakening seismogenic area, in which coseismic ruptures may nucleate and can easily propagate. The rice friction rate parameter a-b is ~0.026, determined by velocity stepping tests (Figure S2a in Supporting Information S1), a dimensionless value comparable to estimates of subduction fault materials parameters at seismogenic conditions (e.g., den Hartog et al., 2012; Rabinowitz et al., 2018). On the contrary, sand shows no or only very minor rate dependence on friction (Figure S2b in Supporting Information S1, Rosenau et al., 2017), causing steady slip and often preventing rupture propagation. The presence of a basal granular layer allows overcoming the possible limitation of high friction affecting previous models, where instead analog faults were created with foam-against-foam surfaces (e.g., Anooshehpoor & Brune, 1994; Brune, 1973]. Our approach is an alternative to the one proposed by Caniven and Dominguez (2021), who covered the foam surface with an epoxy resin. *Foamquake* mimics the key features of a generic natural megathrust and does not aim to reproduce a specific subduction configuration. However, the model can be tuned adding one or more asperities or varying frictional properties of the interface both along trench and downdip. Material properties data are published open access in (Mastella, Corbi, Funiciello, Rosenau et al., 2021).

2.3. Model Scaling

Model parameters can be related to natural parameters thanks to specific scaling factors (e.g., Hubbert, 1937). The geometrical, kinematical, dynamical and rheological behavior of the model must be similar with respect to nature. Through dimensional analysis, we provide dimensionless numbers, describing the significant quantities of *Foamquake* (Table S1 in Supporting Information S1). Our model has been designed with a length scaling factor L^* of $2.9{\cdot}10^{-6}$ (i.e., 1 cm in the model corresponds to 3.5 km in nature). Accordingly, *Foamquake* represents a 510×310 km^2 subduction system when scaled to nature. The downdip width of the seismogenic asperity upscales to 105 km, while its updip- and downdip limits distance from the trench 35 and 145 km, according to the downscaled values of the worldwide average of natural seismogenic zones (Heuret et al., 2011).

For models performed in the natural gravity field (i.e., $g_{nat} = g_{mod}$), the stress scaling factor, σ^* is set comparing model and nature lithostatic stress and is computed with the product of ρ^* by L^*, where ρ^* is the model/nature density ratio. Foam density is ~20 kg/m^3; assuming an average crustal wedge density of 2900 kg/m^3, σ^* is $2.0{\cdot}10^{-8}$ (i.e., 1 Pa in the model is equivalent to 50 MPa in nature). Elastic properties ratio E^* should scale as σ^* as they share the same dimensions. Assuming an average lithospheric E of 10^{11} Pa in nature (Turcotte & Schubert 2014), the E of the analog wedge should be 2 kPa, instead of 30 kPa as for the foam rubber implemented in this study. To compensate for such mismatch and to keep the E^* and σ^* balanced, an extra normal load of a few tens of Pa is required (see Section 3.1).

In real subduction zones, interseismic and coseismic phases are governed by different deformation rates. The coseismic phase is a dynamic phase controlled by inertia and can be described using the Froude number (i.e., ratio between inertia and gravitational forces of a body, e.g., Rosenau et al., 2017). On the contrary, the interseismic phase is governed by non-dynamic (static) frictional and viscous deformation processes. Therefore, two different time scaling factors can be used as originally proposed by Rosenau, Lohrmann, and Oncken (2009). Keeping the Froude number, the same in laboratory and in nature, the time scaling factor for the coseismic phase (T_c^*) is set as the square root of L^* (i.e., 1s in the model upscales to 590s in nature). None of the elements of our model displays viscous behavior, therefore the interseismic phase need not to be dynamically scaled. We arbitrarily define the interseismic scale factor (T_i^*) as $3.1{\cdot}10^{-9}$, that is, 1s in the model upscales to 100 years in nature for obtaining kinematic similarity with the multi-century recurrence times similar to nature. Interseismic and coseismic velocity scaling factors can be calculated by dividing L^* by the respective temporal scale factors. While absence of viscous elements hinders our model to mimic a bulk postseismic relaxation, frictional postseismic creep could occur around asperities. However, this transient is not resolvable due to the monitoring system displacement resolution.

2.4. Monitoring and Data Processing

The monitoring is performed with a high-resolution (2048 x 1536 pixel^2, 8 bit, 256 gray levels) top-view camera capturing images at 50 frames per second (fps). An additional model has been monitored at 100 fps as a benchmark to better highlight the kinematics of foamquakes ruptures. The acquired images have been analyzed employing the particle-image-velocimetry method PIV, using the MatPIV package (Sveen, 2004). The 2D surface velocity field is extracted through cross-correlation between consecutive images, discretized in 18 x 29 interrogation windows. These windows represent measurement points that in ensemble mimic a spatially dense, continuous geodetic network (i.e., laboratory geodesy (e.g., Corbi et al., 2019, 2020; Kosari et al., 2020), with 1 station every 5 cm of the model, equivalent to 17 km spacing between stations in nature. For tracking model deformation, we seeded the wedge surface with black rice markers. The high PIV resolution allows solving both amplitudes of coseismic and interseismic velocities measured between two frames within the model surface at micron resolution.

From surface velocity time series, we used a standardized procedure to identify slip events. We determined coseismic frames applying a picking algorithm to a reference time series extracted from the interrogation window located at seismic asperity center surface projection (Figures 1a–1b). Due to the model configuration, the maximum coseismic slip is always located around the center of the asperity, excluding a potential picking bias. We used the FPEAK MATLAB algorithm to identify emergent peaks from the lower background interseismic velocity (Text S1 and Figure S3 in Supporting Information S1). We use the locking to quantify model behavior during interseismic periods. We defined locking as the ratio between the interseismic cumulative landward displacement and the cumulative displacement related to subduction. This ratio ranges from 0 (i.e., totally delocked system) to 1 (i.e., fully locked system).

2.5. Source-Parameters Derivation

By multiplying PIV velocities by the time between consecutive frames, we obtained the displacement field at the model surface. From the displacement upscaled to nature, we calculated foamquakes source parameters. Due to the shallow dip of the analog megathrust and the nearfield coverage of PIV measurements until the trench, the coseismic displacement pattern measured at surface is quantitatively close to the real slip inverted at depth. Hereinafter, we consider surface displacement and slip as synonyms, despite this assumption causing slight underestimation of moment magnitudes in the order of 0.1–0.2 (Text S2 and Figure S4 in Supporting Information S1). Foamquakes span more than one frame, therefore, we summed the identified coseismic displacement matrices, obtaining a single cumulative displacement map of each analog earthquake (Figure 2d and Figure S12 in Supporting Information S1). Rupture area A is defined as the product of PIV interrogation window size by the number of windows that overcome a given displacement threshold during one event. We considered 1, 5, and 10 m thresholds obtaining minor variation (±10%) in source parameters. We use the 5 m threshold, which provides the most reliable foamquakes scaling in respect to natural interplate earthquakes. The average displacement D is computed as the mean of the trench orthogonal component of displacement considering exclusively the windows located within the rupture contour. From D and A the seismic moment M_0 [N m] is computed as:

$$M_0 = G \cdot D \cdot A \tag{1}$$

where G is $5 \cdot 10^{10}$ [Pa], the average crustal rigidity.

Finally, the foamquake moment magnitude is (Hanks & Kanamori, 1979):

$$\mathrm{M_w} = 2/3 \cdot \log_{10}(\mathrm{M_0}) - 6.03 \tag{2}$$

Multiplying the number of identified coseismic frames to the sampling interval, the event's duration (T) is obtained, while the time between frames with peaks in velocities is defined as the recurrence interval (R_T).

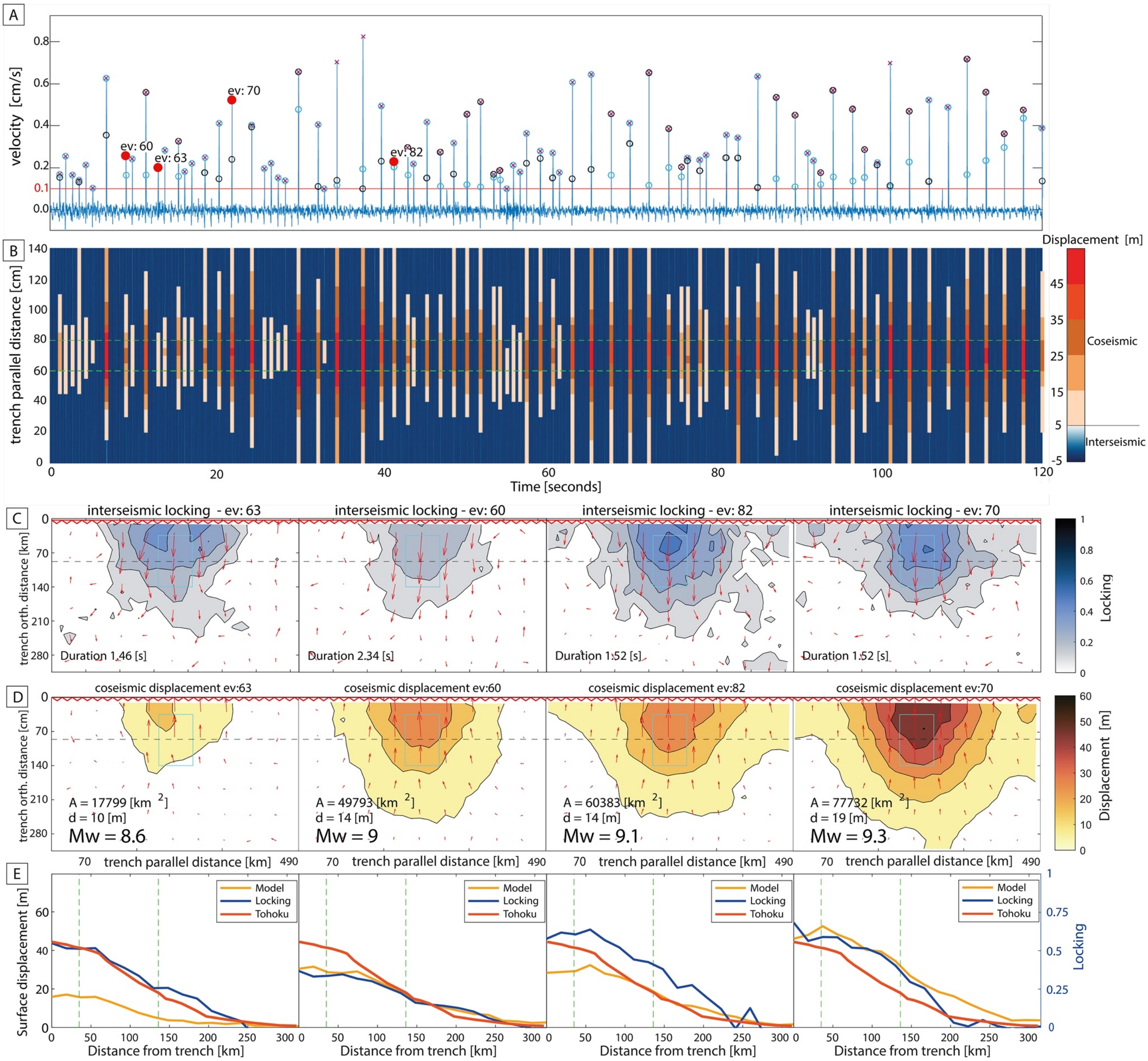

Figure 2. Seismic behavior of 2-min extracted from the reference model (L_w = 20 cm, σ_n = 40 Pa, 15-min long). (a) Velocity time series of the reference point used to identify coseismic events. Values faster than a fixed velocity threshold (red line vs. = 0.1 cm/s) are interpreted as foamquakes. Pink crosses represent coseismic peaks, blue and black circles are first and last coseismic frames, respectively. Filled red circles highlight the 4 foamquakes depicted in (d). (b) Line-time evolution of the model represented by a trench parallel section crossing the downdip center of the seismic asperity. The temporal scale of coseismic stages (i.e., thickness of vertical lines) is exaggerated to improve visibility, while the vertical dimension represents the tench-parallel extent of each foamquake. Green dashed lines depict the limits of the asperity. (c)–(d) Map view details of the 4 seismic cycles. (c) Interseismic deformation patterns: red quivers highlight landward motion of virtual GPS stations, while colormaps depict the superficial interseismic locking (contour levels from 0.1 to 0.5). Quiver spatial density is equal to 1/3 of the available data set. Cyan rectangles represent the velocity weakening asperity. (d) Coseismic displacement maps, contour levels every 10 m (scaled to nature). (e) Trench orthogonal profiles of the superficial coseismic displacement (in orange) and coupling (in blue). In red is depicted the slip pattern for the 2011 M_w = 9.1 Tohoku earthquake inferred by Bletery et al. (2014). Trench-orthogonal profiles are located exactly along the center of the seismic asperity. Vertical dashed lines represent the updip and downdip limits of the asperity.

3. Results

In this section, we first show the general model behavior; then we explain the procedure used for identifying the model configuration that allows reproducing stick-slip cycles scaled with large interplate earthquakes. It has been systematically explored the 2D parameter space formed by the normal load σ_n and the seismic asperity length along trench L_w. We subsequently report the behavior of a 15-min long reference model. This model provides maximum similarities with respect to the natural prototype. Finally, we report results from double asperity models. Experimental data are published open access in (Mastella, Corbi, Funiciello, & Matthias, 2021).

3.1. General Model Behavior

After an initial 1.5 min-phase, characterized by elastic loading of the wedge, the subduction interface starts to exhibit stick-slip dynamics. The initial loading phase, which characterizes seismotectonic analog (Caniven & Dominguez, 2021; Corbi et al., 2013; Rosenau, Lohrmann & Oncken, 2009) and numerical models (Barbot, 2019), has been ignored in the following analysis. Subsequently, the model alternates phases of apparent quiescence (i.e., interseismic) with rapid episodic slip events. During interseismic stages, the friction along the base of the foam rubber results in the mechanical coupling that partially locks the subduction interface. As a consequence of the continuous convergence of the foam wedge, the upper plate moves toward the backstop (i.e., landward; Figure 2c). When shear stress overcomes the frictional resistance of the analog megathrust, a spontaneous instability nucleates, resulting in trenchward (i.e., seaward) motion of the wedge (Figure 2d). In general, spatially and temporally heterogeneous locking is observed with the highest values of 0.4–0.8 above the seismic asperity (Figure 2c).

3.2. Model Sensitivity to Normal Load and Asperity Length

20 models have been performed to investigate how both the asperity along-trench length (L_w) and the external normal load (σ_n) tune the seismic behavior of *Foamquake*. We modulated σ_n adding a given quantity of rice above the foam wedge on the superficial projection of the asperity (Figure 1). Rice grains are too big to penetrate and contaminate the foam and at the same time serve as speckles. We tested five L_w, from 10 to 80 cm, a range scaled to nature from 35 to 280 km. For each L_w, four models have been performed changing σ_n above the asperity, from 10 to 100 Pa, with a step of 30 Pa. Each model runs for 2 min, during which 19–112 foamquakes (depending on model configuration) are detected for a total of 1,062 events. The vast majority of foamquakes are trench breaking (Lay et al., 2012), while non-trench-breaking partial ruptures characterize models with small L_w and σ_n.

Slip episodes recurrence R_T, duration E_D, and size of events with average coseismic displacement (D) and seismic moment M_0 as well as their variability are calculated. To quantify the variability of foamquakes size, we refer to the range of M_w measured for each model, while the temporal variability has been evaluated through the Coefficient of Variation (CoV) of R_T. This coefficient is often used for describing earthquake recurrence periodicity. CoV is a dimensionless parameter describing the dispersion of a selected variable. Considering a seismic catalog, it is defined as the standard deviation divided by the mean recurrence interval. CoV = 0 indicates a perfectly periodic system, whereas a CoV = 1 represents a time-independent Poissonian behavior. In paleo-seismic literature, records with a CoV > 1 are called clustered (McCalpin, 2009), or bursty (Salditch et al., 2020). Intermediately, records with a CoV > 0.5 are defined "aperiodic," while a CoV < 0.5 defines quasi-periodic records (e.g., Kuehn et al., 2008). In our sensitivity study CoV is in the 0.19–0.5 range, testifying a quasi-periodic behavior.

L_w exerts a crucial influence governing the frictional evolution of experimental models. Increasing L_w results in larger and less frequent events (Figure 3). For example, fixing $\sigma_n = 100$ Pa, the model with $L_w = 10$ cm (35 km in nature) includes 81 foamquakes ($R_T = 1.5 \pm 0.4$s; 1σ standard deviation), with an average coseismic displacement D of 9.3 ± 3.3 m, while the $L_w = 80$ cm (280 km in nature) model encompasses only 24 events ($R_T = 4.9 \pm 1.4$s) with a $D = 59.9 \pm 23.0$ m. Longer patches favor higher displacements and larger rupture areas, resulting in higher seismic moments (Figures 3a–3b). The longest patches imply the presence of full ruptures spanning the whole model along strike (Figure 2b). The range of magnitudes ($M_{w\text{-max}}$–$M_{w\text{-min}}$) remains approximately stable (between 0.5 and 1) considering each experimental configuration (Figure 3). This means that while the average magnitude scales with L_w, the magnitude range (i.e., the variability for the tested configurations) is independent of L_w.

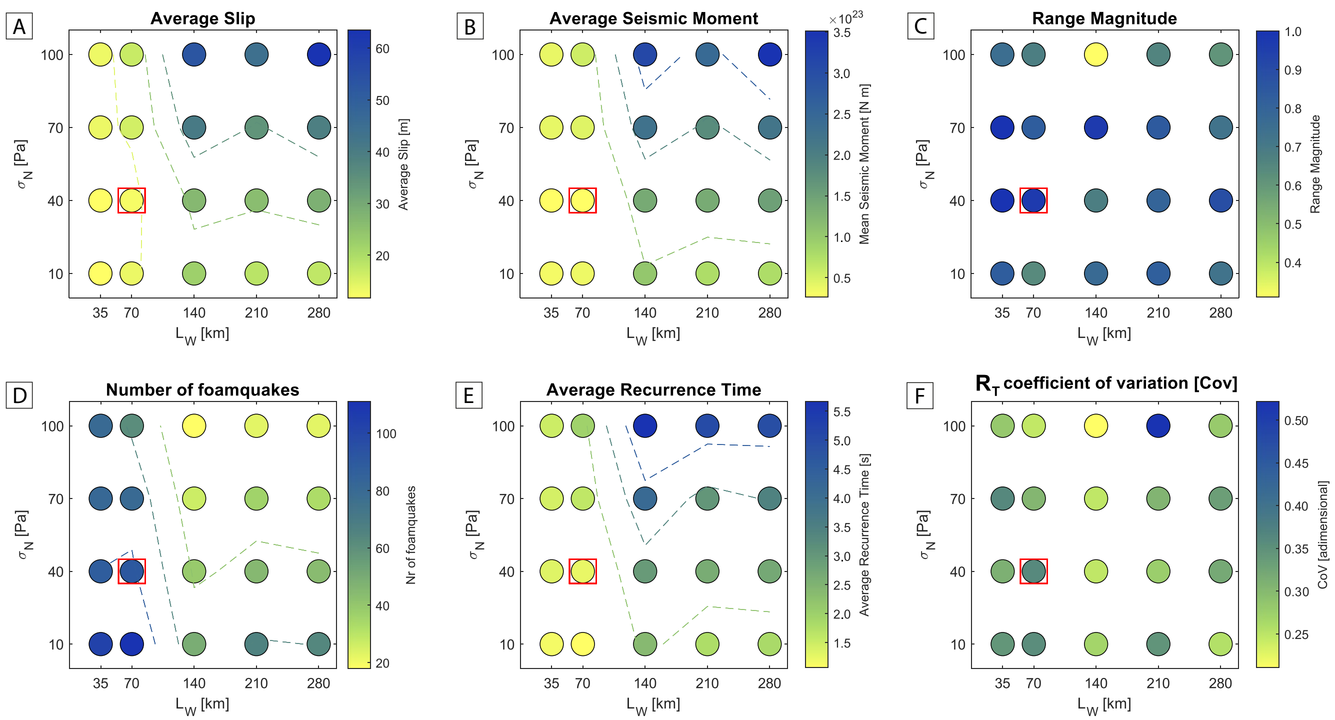

Figure 3. Fomquakes properties represented for each performed model, varying L_w and the normal load above it (σ_n). Red rectangles highlight the reference model with $\sigma_n = 40$ Pa and $L_w = 20$ cm (70 km scaled to nature).

The increase of σ_n above the seismic asperity controls the spatiotemporal sliding behavior of our models. Higher σ_n promotes larger events, both in terms of average slip and average rupture area (Figures 3a–3b). Accordingly, also the event duration T increases (Figure 4), while the number of foamquakes decreases, resulting in longer seismic cycles (Figure 3d). For $L_w = 20$ cm and $\sigma_n = 100$ Pa, the experimental catalog includes 62 events ($R_T = 1.9 \pm 0.5$s), half of the number observed with the same L_w but $\sigma_n = 10$ Pa ($R_T = 1.1 \pm 0.4$s). For low σ_n and small L_w, the system alternates distinct families of recurrence intervals, which are multiples between them (i.e., period-doubling behavior; Kato, 2014; Ma & He, 2001; Mele Veedu et al., 2020; Shelly, 2010).

The analysis of foamquakes sizes for each configuration allowed identifying the model with $\sigma_n = 40$ Pa and $L_w = 20$ cm as the best-scaled configuration. This model produces analog earthquakes with up to 9m as average displacement when scaled to nature. Hence, *Foamquake* does not produce only stick-slip dynamics but also slip phases whose size properly scales with the slip of natural interplate earthquakes. This configuration has been further examined performing a 15-min model, considered as the reference model and described in the next section.

3.3. Earthquake Behavior of the Reference Model

505 foamquakes occur in the reference model. The average displacement of individual foamquakes ranges from 18 to 78 μm (6.6–28 m when scaled to nature). Considering all seismic ruptures, the average is 15.7 ± 2.6 m. The associated seismic moment average is $M_0 = 4.9 \cdot 10^{22} \pm 2.9 \cdot 10^{22}$N m, equivalent to a magnitude $M_w = 9.0 \pm 0.2$. Coseismic phases last from 0.02 to 0.08s, that is, the duration of 1–4 consecutive frames. Within the temporal resolution, we observe a direct proportionality between event duration and magnitude. Recurrence periods range between 0.62 and 2.52s (i.e., ideally 62–252 years when scaled to nature), with an average of 1.63 ± 0.54s and are branched into three distinct groups as shown in Figures S14c and S14d in Supporting Information S1. The reference model alternates long (∼2.25s), intermediate (∼1.2s), and short (∼0.6s) repeat periods. Figure S5 in Supporting Information S1 shows that recurrence periods are proportionally correlated with magnitude.

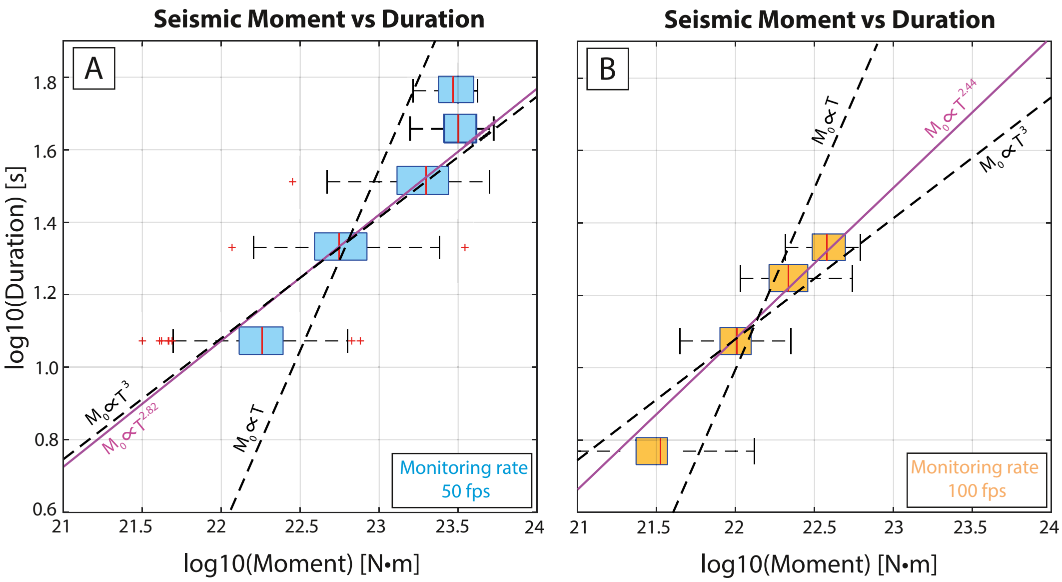

Figure 4. (a)–(b). Seismic moment *vs.* duration from models monitored at 50 fps (a) and from models monitored at 100 fps (b). Seismic moments values for each subset of durations are represented through a boxplot, where the central red mark indicates the median, the box edges indicate the 25th and 75th percentiles, the whiskers extend to the most extreme value of that subset not considered outlier, while outliers are plotted individually with the red‘ + marker. Pink lines ($M_0 \propto T^{2.82}$ and $M_0 \propto T^{2.44}$) are the best-fitting regression lines obtained through a grid-search inversion, compared with cubic scaling of regular earthquakes (dashed lines $M_0 \propto T^3$) and linear scaling of slow slip earthquakes (dashed lines $M_0 \propto T$). All foamquakes quantities are scaled to nature.

3.4. Double-Asperity Models

The dimension of *Foamquake* allows investigating the along-trench propagation of ruptures and, in turn, to highlight how the along-trench frictional segmentation affects the seismic behavior. We performed four additional models with two asperities, both sized $L_w = 20$ cm and $W = 30$ cm (i.e., the same size as in the reference model), distanced by 40 cm (140 km in nature). We fixed $\sigma_n = 40$ Pa above one asperity (as in the reference model, accordingly named reference asperity), while we varied σ_n above the other asperity (hereafter named secondary asperity), from 10 to 100 Pa, with 30 Pa steps.

The model generates single- and double-asperity ruptures. The former includes ruptures that nucleate within an asperity, propagate partially along the barrier but arrest before involving the second asperity. The second includes foamquakes with two asperities failing during the same event (i.e., asperity synchronization). The coexistence of single- and double asperity ruptures causes a larger variability of source parameters with respect to the reference model.

Here we describe the recurrence behavior of double asperities models using the model with both asperities with $\sigma_n = 40$ Pa as a proxy. We select 4.2 s of the 2 min-long model, during which six foamquakes have been captured (Figure 5). Events 26, 27, and 30 are single-asperity ruptures, with magnitude between 8.6 and 9.2. On the other hand, examples of asperity synchronization are events 28, 29, and 31. Those ruptures generally nucleate in one asperity and subsequently involve the central barrier and the other asperity (e.g., event 31-Figure 5d).

To distinguish single-versus double-asperity ruptures and quantify their relative proportion, we applied a density-based temporal clustering algorithm, DBSCAN (Ester et al., 1996), capable of grouping coseismic frames relative to multi-asperities ruptures (Text S3 in Supporting Information S1 for details). We found that the number of foamquakes with asperities synchronization decreases as a function of σ_n of the secondary asperity (Figure S8 in Supporting Information S1). In particular, 91% of foamquakes are double-asperity ruptures for the model with $\sigma_n = 10$ Pa, while only 51% of events represent synchronized asperities ruptures for the model with $\sigma_n = 100$ Pa. The total number of events follows an inverse trend, increasing from 131 to 155 considering these two models. Double-asperity ruptures are more frequent with low σ_n and show larger displacement and magnitude in respect

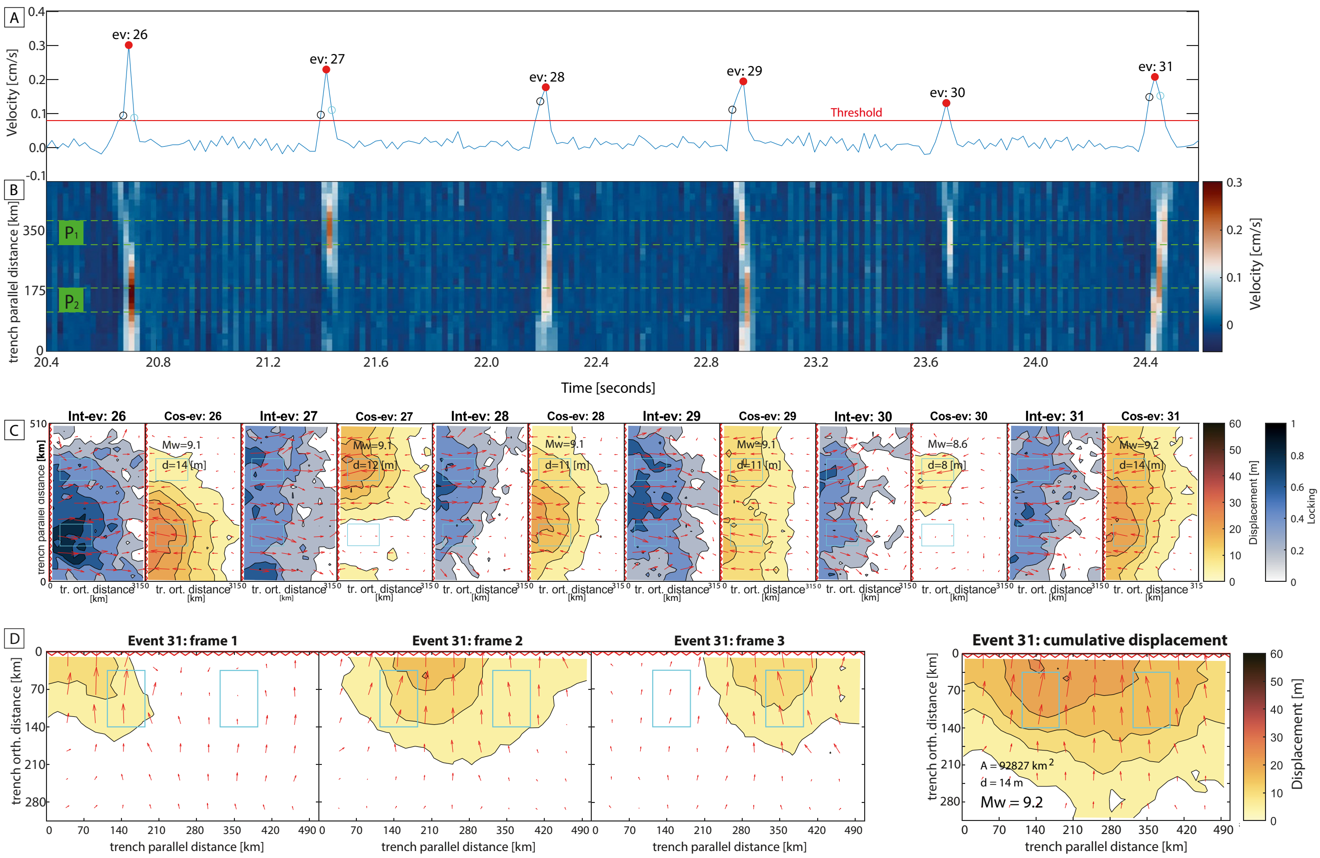

Figure 5. Representation of 4.2 s of the reference double asperity model (L_w = 20 cm, σ_n = 40 Pa) (a) Particle-image-velocimetry maximum superficial velocity time series (b) Line-time evolution of the model obtained through a trench parallel section crossing the downdip center of seismic asperities. Green dashed lines depict the limits of asperities (c) Representation of interseismic locking maps and subsequent coseismic cumulative displacement maps for each seismic cycle (d) Rupture propagation of event 31: Rupture starts within the left asperity and then propagates involving in a second moment the other asperity.

to single-asperity ruptures from the same model (Figures S9 and S10 in Supporting Information S1). Generally double-asperity ruptures nucleate in the asperity with the lower σ_n and subsequently trigger the other asperity (Figure S11 in Supporting Information S1).

Except for the model with σ_n = 10 Pa above the secondary asperity, single-asperity ruptures involve more frequently asperities with the lower σ_n. Conversely, σ_n seems not to control the displacement amplitude of single-asperity ruptures. Increasing σ_n (of the secondary asperity) does not increase foamquakes magnitudes and displacements as instead observed in single asperity models (Figures S9 and S10 in Supporting Information S1).

Double-asperity models systematically experience a larger number of foamquakes than single-asperity models, according to the presence of two seismogenic sources. The system is still characterized by period doubling-behavior, with distinct families of R_T. CoV of R_T is in the 0.15–0.27 range, indicating a quasi-periodic recurrence behavior similar to single-asperity models. Figure 6 shows that both the reference and the secondary asperity experience shorter cycles (R_T) with respect to the corresponding single asperity model cycles durations. This observation is particularly clear due to the presence of distinct classes of R_T. For example, the R_T of the double asperity model with the secondary asperity with σ_n = 100 Pa includes only a few interseismic periods of ~2.25s (Figure 6), that instead are the most frequent R_T in the corresponding single-asperity model (Figure 6l).

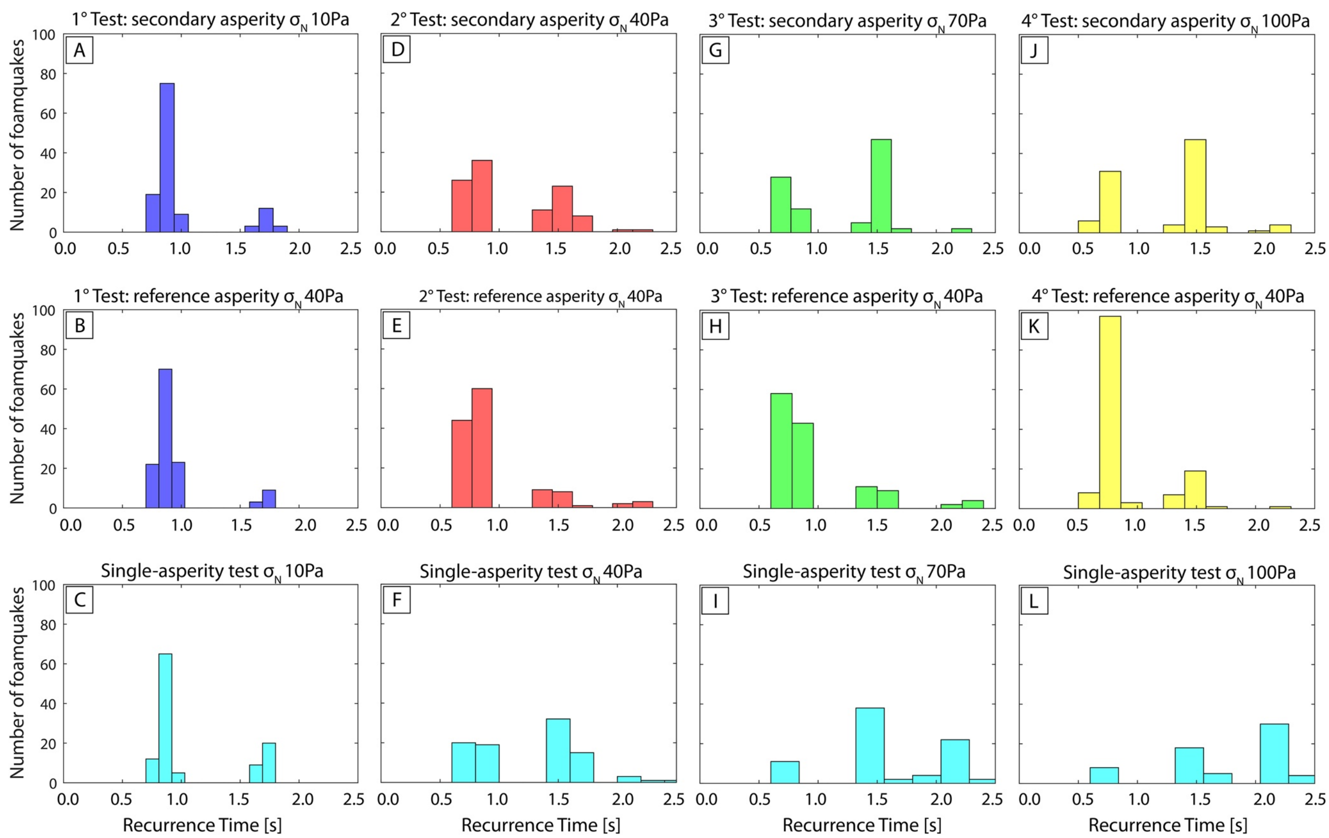

Figure 6. Comparison of foamquakes recurrence time (R_T) histograms between double- (A-B-D-E-G-H-J-K) and single asperity models (C-F-I-L). The first two rows refer to R_T of double asperity models: the second row represents R_T of the reference asperity ($\sigma_n = 40$ Pa), while the first is the R_T of the asperity with variable σ_n (from 10 to 100 Pa). The third row in cyan, corresponds to single asperity models.

4. Discussion

4.1. Single-Asperity Models

Several parameters have been proposed to explain the variability of seismic behavior of different subduction zones (e.g., Heuret et al., 2011; Schäfer & Wenzel, 2019; Schellart & Rawlinson, 2013). Frictional and geometrical properties of asperities together with their spatial distribution control the trench-parallel length along which a seismic rupture is capable of propagating (e.g., Corbi, Funiciello et al., 2017; Dublanchet et al., 2013; Kaneko et al., 2010; Rosenau et al., 2019). Another important role in controlling interplate seismicity is played by geological features, such as the presence of ridges and seamounts (e.g., Bilek, 2007; Contreras-Reyes & Carrizo, 2011; van Rijsingen et al., 2018] or sediment thickness at trench (Brizzi et al., 2020; Heuret et al., 2012). These features may influence the stress field at subduction zones and the normal load acting on megathrust segments (e.g., Scholz & Small, 1997). Elevated normal stress on seismic asperities introduces nontrivial recurrence behavior and allows for higher stress drops even along a relatively simple fault configuration (e.g., Lui & Lapusta, 2018).

In our model as σ_n increases, and in turn also the yield strength of a given asperity increases, larger and less frequent foamquakes are observed. These results reflect the strong dependence of the recurrence time on normal stress, as described by the basic Coulomb friction model. In that model (R_T) = (stress drop)/(shear stressing rate) and stress drop is proportional to normal stress. Consequently, also R_T is proportional to σ_n. This evidence is also theorized by rate and state laws (e.g., Barbot, 2019; Dieterich & Linker, 1992; Mele Veedu & Barbot, 2016; Okubo & Dieterich, 1984; Wang & Scholz, 1994) and agree with rock mechanics observations from double direct shear apparatus experiments (e.g., Scuderi et al., 2016). In *Foamquake*, the seismic behavior is also controlled by the trench-parallel extent of asperities. Longer asperities favor bigger and less frequent events. A primary control on maximum earthquake size exerted by the trench-parallel dimension available for ruptures to grow is intuitively a basic implication of elasticity and agrees with statistical inferences from worldwide subduction zones (Brizzi et al., 2018).

Varying L_w and σ_n we identified the configuration ($L_w = 20$ cm and $\sigma_n = 40$ Pa) that better scales with the natural prototype. Although in this model we cannot observe foamquakes smaller than $M_w = 8.2$, the coseismic displacement amplitude is adequately scaled to natural subduction earthquakes. This result represents a step forward in respect to several seismotectonic models. Indeed, previous studies applied a specific scaling factor for the coseismic slip (e.g., Caniven & Dominguez, 2021) or found some turn-around to calculate analog earthquake magnitudes (Corbi, Funiciello et al., 2017; Rosenau, Lohrmann & Oncken, 2009).

Despite unavoidable model limitations (Section 2 and Text S4 in Supporting Information S1), it is tempting to compare foamquakes obtained from the reference single-asperity model to the 2011 $M_w = 9.1$ Tohoku earthquake (Tsuda et al., 2017), which is the best instrumentally monitored mega-earthquake ever occurred. Some foamquakes, such as events 60 and 82 in Figures 2d and 2e are characterized by source parameters (average slip of 14m and an average rupture area between $\sim 5 \cdot 10^4$ and $6 \cdot 10^4$ km^2) comparable to the Tohoku earthquake source parameters (e.g., Satake et al., 2013). Figure 2e depicts trench-orthogonal profiles of the surface coseismic motion. Foamquakes exhibit an asymmetric bell-shaped profile akin to the Tohoku earthquake. Analog profiles show a general amplitude and seaward displacement decay comparable to the slip model of Bletery et al. (2014), which includes near trench observational constraints.

4.2. Source Parameters: Foamquakes Versus Large Interplate Earthquakes

Scaling relations between subduction earthquake parameters illuminate the physics of seismogenesis. Several scaling relations have been proposed for subduction earthquakes (e.g., Blaser et al., 2010; Murotani et al., 2008; Strasser et al., 2010). Their main difference is generally related to uncertainties in the inversion of geodetic and waveform data used to calculate source parameters. Other odds depend on the inclusion of aftershocks data to define some relations (Blaser et al., 2010; Strasser et al., 2010). Murotani et al. (2013) compiled source parameters for seven giant ($M_w \sim 9$) earthquakes globally distributed for which the heterogeneous slip distributions were estimated from tsunami and geodetic data, adding 25 slip models of 10 great earthquakes ($M_w > 8.5$, excluding aftershocks). Here we compare these scaling laws with those from *Foamquake* to provide a quantitative estimation of model similarity with respect to the natural prototype. Murotani's models are indicated for the purpose as the magnitude of foamquakes is always higher than 8.2. Moreover, Murotani's catalog also encompassed recent great earthquakes like the Maule and the Tohoku-oki earthquakes. The Murotani's regression models respect to the seismic moment M_0 are listed below: for the rupture area [km^2] $A = 1.34 \times 10^{-10} \cdot M_0^{2/3}$, for the average slip [m] $D = 1.66 \times 10^{-7} \cdot M_0^{1/3}$ and for the asperity area [km^2] $A_S = 2.81 \times 10^{-11} \cdot M_0^{2/3}$, where M_0 is defined in N·m.

From our data set, scaling laws have been determined for these couples of parameters: M_0 versus rupture area A, M_0 versus average slip D, and M_0 versus asperity size A_s. We defined the asperity area as the area of the rupture with coseismic slip 1.5 higher than the average slip D of the rupture, as in Murotani et al. (2013). This definition excluded a few (i.e., 2.2%) events, for which no sub-faults overcame the 1.5D threshold, precluding the possibility to define a spatial asperity.

We estimated scaling parameters through linear fitting, considering the function:

$$\log_{10}(X) = a + n \cdot \log_{10}(M_0) \tag{3}$$

Described by two unknown parameters: the dimensionless coefficient a, and the seismic moment exponent n. The seismic moment exponent is the most indicative parameter; for example, regarding the rupture area relation, n represents a first order evaluation of the rupture mode, being related to the difference between circular crack and pulse-like models of earthquake growth.

Foamquakes scaling of moment versus rupture area shows almost the same exponent (~0.68) in respect to the Murotani et al. (2013) scaling $A \propto M_0^{2/3}$. Slip versus moment fit follows a $A \propto M_0^{0.25}$ proportionality, slightly different from the 1/3 exponent observed in nature. The best-fitting analog moment exponent for the asperity area versus M_0 relationship is 0.45, ~30% smaller than the ⅔ scaling of natural mega-earthquakes (Figures 7). Generally, the scaling law goodness of fit does not change modifying any of the experimental conditions. This suggests that the underlying physics controlling foamquake ruptures propagation is independent of changes in σ_n or L_w.

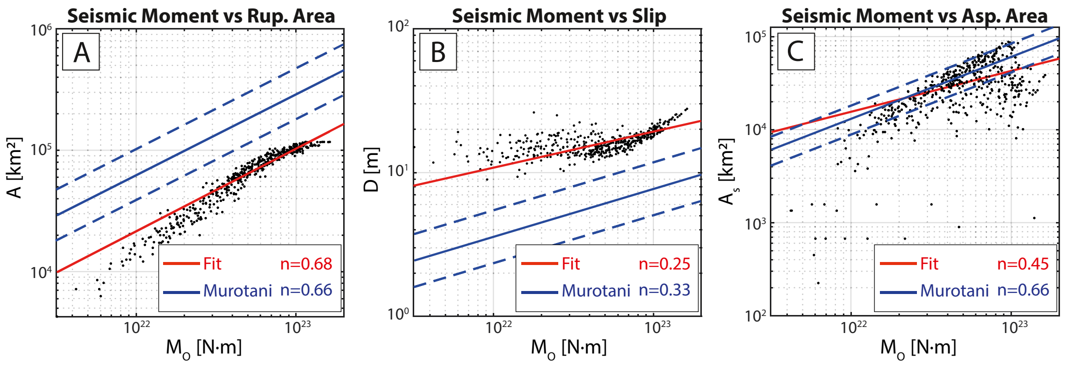

Figure 7. Comparison between foamquakes source parameters and large interplate earthquakes scaling (Murtonai et al., 2013). Seismic moment versus rupture area (a), moment versus average displacement (b) and moment versus asperity area (c) scaling of foamquakes (red lines) compared to the scaling of natural interplate earthquakes (blue line, dashed lines are 1 σ uncertantanties). Best fitting exponents for foamquakes are reported and compared to Murotani's values, considering the form $X \propto M_0^{2/3}$.

From rupture area and moment, we calculated the stress drop associated with each foamquake, applying the circular crack model, a dynamical model that fits most properties of seismic ruptures to first order ($M_0 = C\Delta\tau A^{3/2}$, where $\Delta\tau$ is the stress drop and C is a constant equal to 2.44; Kanamori & Anderson, 1975). The empirically estimated stress drops range from 2 to 40 MPa when scaled to nature. This range is similar to stress drops of giant subduction earthquakes, such as the Tohoku (Hasegawa et al., 2011) and the Maule earthquakes (Luttrell et al., 2011).

Another fundamental scaling law is given by the relationship between seismic moment and slip duration. The underlying idea is that duration is proportional to the moment for slow earthquakes (Houston, 2001; Ide et al., 2007; Peng and Gomberg, 2010), while for regular earthquakes duration scales as the cube root of seismic moment. The scaling difference has been widely interpreted (e.g., Dal Zilio et al., 2020; Ide et al., 2008; Gomberg et al., 2016), mainly assuming different physics of earthquake growth, but it has been considered also as an artifact related to slow slip catalogs from different megathrust zones (Michel et al., 2019).

Moment and duration of foamquakes have been compared to identify their scaling. To strengthen our observations, we analyzed both the models monitored at 50 and 100fps. Figures 4a and 4b depicts the best-fitting relation between seismic moment and duration of foamquakes. Foamquakes follow an $M_0 \propto T^{2.82}$ and $M_0 \propto T^{2.44}$ proportionality considering models monitored at 50fps and 100fps respectively. Moment-duration proportionality of foamquakes thus appears independent of the monitoring rate. Both best-fitting duration exponents are slightly smaller (~5% and 22%) than the $n = 3$ exponent characterizing natural earthquakes. On the contrary, the $n = 1$ exponent is strongly unlikely, giving a large increase (i.e., ~160%) in the RMSE minimization parameter. This observation supports the mechanical and dynamical similarity between foamquakes and earthquakes in nature.

4.3. Along Trench Frictional Segmentation: Double-Asperity Models

The along-trench frictional segmentation of subduction megathrusts is supposed to play a significant role in controlling their seismic behavior (e.g., Lay & Kanamori, 1981). Wide and strongly velocity strengthening regions are thought to act as permanent barriers for the along-trench rupture growth and, in turn, to limit earthquake magnitude (Kaneko et al., 2010). Viceversa, tightly spaced asperities surrounded by weak barriers represent favorable conditions for multi-asperity ruptures and for the genesis of mega-earthquakes. Examples of multiple asperities events include the 1960 Chile earthquake ($M_w = 9.5$; Moreno et al., 2009) and the 2004 Sumatra-Andaman earthquake ($M_w = 9.2$; Subarya et al., 2006). Both numerical (Dublanchet, 2019; Kaneko et al., 2010) and analog models (Corbi, Funiciello et al., 2017; Rosenau et al., 2019) showed that the probability of asperities synchronization depends on physical and geometric properties of barriers and asperities.

Here this type of investigation is extended with *Foamquake*. We analyzed a configuration constituted by two asperities with the same geometrical and frictional properties, distanced by a fixed length (i.e., 2 times the indi-

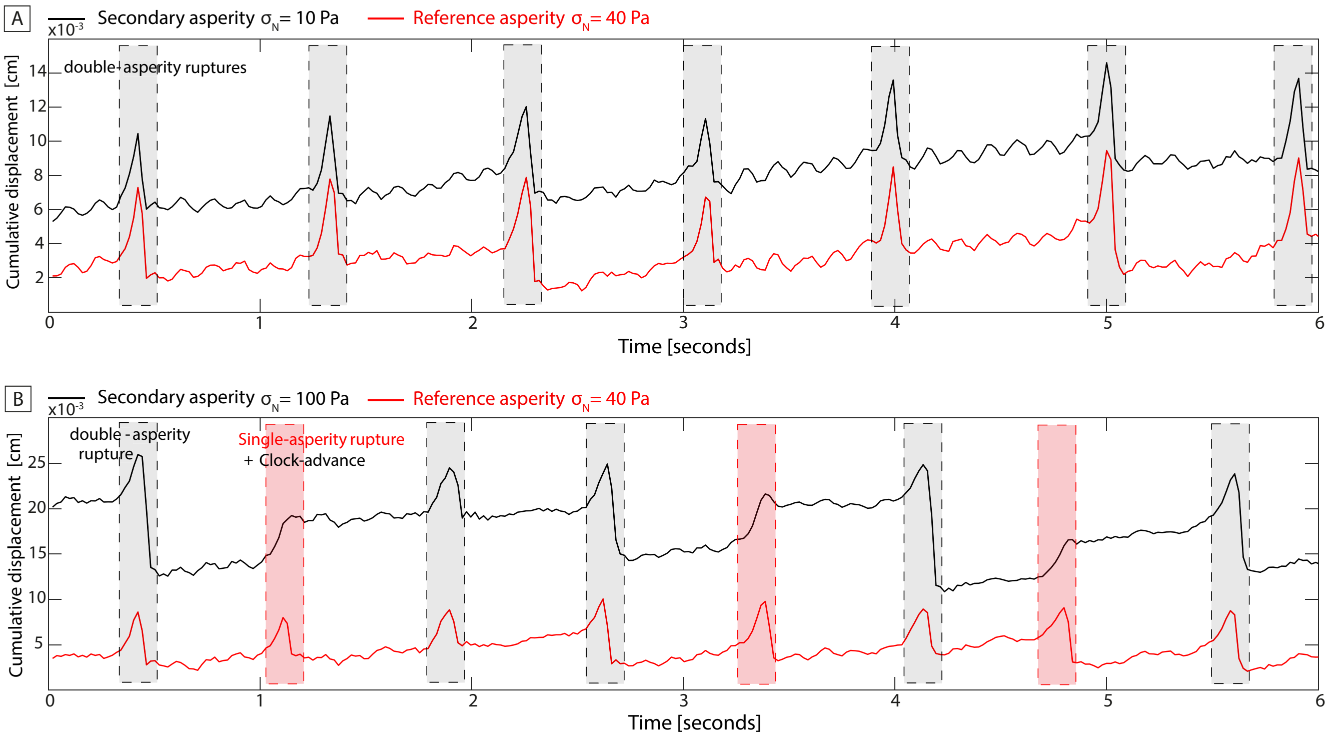

Figure 8. Interaction between asperities with different σ_n. Cumulative velocity time series from two reference points located above the two seismic asperities centers. The reference asperity (σ_n = 40 Pa) is the red one. (a) Model with σ_n = 10 Pa above the secondary asperity. All ruptures are synchronized, as highlighted by gray rectangles. (b) Model with σ_n = 100 Pa above secondary asperity. Single- and double-asperity (red rectangles) foamquakes coexist together.

vidual asperity length), varying the σ_n above them. Double-asperity models exhibit single-asperity earthquakes alternating with double asperity ruptures (Figure 5). Figure 6 shows that both asperities are characterized by shorter R_T compared to the corresponding single asperity model cycles durations, confirming that the interaction of 2 neighbor asperities causes a "clock advance" temporal effect (e.g., Ruff 1996).

The number of synchronizations depends on σ_n above each asperity. σ_n controls the recurrence of a given asperity, as observed in single-asperity models. Figure 8 depicts cumulative velocity time series of two asperities, with a σ_n = 10 Pa above the secondary asperity (in red). Since both asperities are characterized by a small frictional resistance, they fail almost systematically (i.e., 91%) simultaneously. The weaker asperity dictates the system recurrence periods (Figure 6) according to Rosenau et al. (2019). Figure 8 depicts the case with a σ_n = 100 Pa above the secondary asperity. Given its lower σ_n, the reference asperity experiences more events. When this asperity ruptures, it promotes an accelerating transient along the model, but not always the acceleration is strong enough to force the secondary asperity to overcome its frictional resistance and slip together (Figure 8b). This observation suggests that the "permeability" of a barrier depends not only on its frictional strength (e.g., Dublanchet et al., 2013; Kaneko et al., 2010) but also on the physical properties of the two asperities. σ_n of the secondary asperity controls the proportion of single-to double asperities ruptures and also the nucleation of double asperities ruptures: ruptures tend to nucleate in the asperity with the lower σ_n and trigger the other asperity to fail coseismically in a later moment (Figures S11 and S12 in Supporting Information S1) Interestingly, this tendency agrees with experimental results observed in strike-slip analog models (Caniven et al., 2017).

Below, we show that *Foamquake* succeeds in reproducing the first-order peculiarities of the space-time rupture history over multiple seismic cycles of several megathrust segments. We focus on similarities and differences with three subduction zones that share similar patterns and where a historical record of multi-cycle ruptures is available: the Sanriku-Tohoku segment (e.g., Satake, 2015) and the Nankai Trough of the Japan-Kuril Trench (Fujiwara et al., 2020; Garrett et al., 2018; Kitamura et al., 2018; Kodaira et al., 2006) and the Conception and Valparaiso segments along the Chilean margin (Beck et al., 1998; Carvajal et al., 2017; Melnick et al., 2009). Those three subduction zones are characterized by a similar long term space-time rupture pattern: the superimposed cycles rupture behavior (Philibosian & Meltzner, 2020). This behavior involves two or more neighboring segments with similar or different R_T, and/or rare multi-segments ruptures. Frequent barriers separate frictional segments that have failed individually at least once in historical time. Sometimes barriers are "permeable" leading to the failure of multiple segments in a synchronized fashion. In the long-term, subduction segments may show complementary ruptures, during which single-segment earthquakes involve different sections in a sequential fashion.

Superimposed cycles embed nested "serial ruptures" (Atwater & Griggs, 2012), also called ruptures cascades (Philibosian & Meltzner, 2020). In this pattern, the interseismic strain accumulation is released in a temporally clustered series of earthquakes on neighboring frictional segments. Cascade sequences can last from hours to months or even years and ruptures may involve separated or overlapped megathrust segments. Clear examples of cascades include for example : the 2010 Maule ($M_w = 8.8$) and Illapel ($M_w = 8.3$) earthquakes, which occurred distanced by 6 months along the separated segments of Conception and Valparaiso in Chile (Melnick et al., 2017) or in a much shorter timing, the 1854 twin earthquakes Ansei I and Ansei II, occurred at Nankai trough with 32 hr delay (Ando, 1975).

The space-time recurrence behavior of *Foamquake* is comparable to rupture-patterns presented above. We consider double-asperity models analogous to an along trench frictionally segmented megathrust. In our model the barrier separating two asperities can be partially involved by single-asperity ruptures (e.g., event 27 in Figure 5) or sometimes is completely overcome during double-asperity events (Events 28 and 29 in Figure 5). Single-asperity ruptures can be part of long-term complementary rupture sequence, during which the static stress interaction due to a single-asperity event favors a subsequent slip within the neighbor asperity in the next foamquake. As a result, these multi-cyclic ruptures sequentially involve the whole along-trench model dimension (e.g., events 26-27-28 in Figure 5).

Events 29 and 31 in Figure 5 represent examples of short-term, coseismic rupture cascades: the rupture nucleates in one asperity and propagates along-trench involving the neighbor asperity in a second moment. Similar patterns have been observed in gelatine seismotectonic models (Corbi, Funiciello et al., 2017) and in numerical simulations (Kaneko et al., 2010). As an example, it is reported the comparison between event 22 of the model with $\sigma_n = 100$ Pa above the secondary asperity and the 2016 Pedernales earthquake ($M_w = 7.8$), where two patches ruptured sequentially in distinct phases during one minute of rupture propagation (Figure S12 in Supporting Information S1; Nocquet et al., 2017).

Our double-asperity models highlight the key role of "permeable" barriers, which introduce irregularity in the recurrence behavior of a given trench segment, as proposed by Konca et al. (2008), and suggested by dynamic rupture modeling (Ben-Zion & Rice, 1993; Cochard & Madariaga, 1996). This observation supports the idea that long earthquake chronologies are required to properly characterize the earthquake recurrence variability of subduction segments (Philibosian & Meltzner 2020).

4.4. Recurrence Behavior, Experimental Variability and Repeatability

Our models, both with one and two asperities, are characterized by CoV in the 0.19–0.5 range, expression of a quasi-periodic recurrence behavior. This evidence agrees with observations from other seismotectonic models (Corbi et al., 2013; Rosenau & Oncken, 2009). On the contrary, Brune et al. (1990) found a strong periodicity of slip phases in their foam models, with a CoV of 0.1. Similarly, elastic sliders by Corbi et al. (2011) show a regular recurrence in terms of size and period of events. This difference can be easily explained by the 3D nature of *Foamquake* associated with the coexistence of partial- and full ruptures, introducing spatially heterogeneous rupture histories.

In real subduction zones, the CoV is generally obtained from paleoseismic investigations. Well-dated geologic indicators, such as coral microatolls (e.g., Natawidjaja et al., 2006; Philibosian & Meltzner, 2020), lacustrine (e.g., Moernaut et al., 2014) and marine turbidites (e.g., Noda et al., 2008; Satake & Atwater, 2007), offer a powerful tool to investigate long recurrence records. Quasi-periodic earthquakes have been inferred in Sumatra (Natawidjaja et al., 2004), South Chile (Bookhagen et al., 2006), Cascadia (Kulkarni et al., 2013), Alaska and New Zealand (Lajoie, 1986).

The CoV parameter in nature could depend on the completeness and resolution of catalogs: Its value could be potentially biased due to the short extension of paleo-seismic catalogs (e.g., Goes, 1996) or to some artifacts of different paleoseismic methods (e.g. Goldfinger et al., 2012; Stein & Newman, 2004). The same problem may concern our 2-min long models. Therefore, we decided to verify whether our foamquake catalogs had enough intervals to provide reliable recurrence histories. For each model, we calculated the CoV increasing the number of recurrence intervals until using the whole time series. We analyzed how many foamquakes are required to stabilize the CoV at a constant value. We arbitrarily considered a CoV as constant if it remains within a range of ± 0.1 removing the last five intervals of each record, similarly to what has been assumed for paleoseismic records by Moernaut (2020). Additionally, we performed the same procedure randomly resampling the records 100 times, producing a total of 2,000 synthetic records. Considering all the simulations, we calculated the number of events needed to stabilize the CoV within the ranges ± 0.1, and $\pm 20\%$ of the total value. We found that all synthetic seismic catalogs are statistically reliable, given that removing the last five intervals, the calculated CoV remains in the ± 0.1 range considering the real CoV (Figure S13 in Supporting Information S1). This evidence agrees with what is observed in lacustrine paleoseismic records (Moernaut, 2020), where at least 10 intervals are needed to allocate a record to the main recurrence model based on the CoV.

Moreover, we evaluated if our records can be associated with a time-independent Poissonian model, characterized by an exponential distribution of recurrence intervals. To reject this hypothesis, we applied the Lilliefors test, a two-sided goodness-of-fit test suitable when the population parameters are unknown (Lilliefors, 1969), increasing the number of foamquakes considered. The minimum number of foamquakes needed to reject the exponential distribution for each model ranges from 5 to 10, demonstrating that our 2 min-long models are unbiased by record length and can successfully reflect the real recurrence behavior of the investigated stick-slip process.

To strengthen our study and provide a quantification of model repeatability, we executed two additional 15 min-long models, reproducing the reference configuration (σ_n = 40 Pa and L_w = 20 cm). We investigated if longer models own a similar statistic in respect to shorter models. First, we compared the recurrence behavior by the mean of the CoV. We compared the CoV of the shorter model to the CoV calculated in 2-min temporal shifting windows within the longer test. In the longer test, the CoV varies within a small range (0.26–0.42) and sometimes equals the value derived from the 2 min model (CoV = 0.36; Figures S14c and S14d in Supporting Information S1). Moreover, we randomly subsampled 1,000 sub-catalogs from the longer test, evaluating each time the CoV. Also in this case, the observed variability encompassed the value of the shorter test (Figures S14a and S14b in Supporting Information S1). Then, we selected seven properties of foamquakes to be quantitatively compared between long and short experiments: seismic moment, rupture area, average slip, magnitude, stress drop, recurrence time, and foamquakes duration. We examined the average and two standard deviations of all parameters. Despite slightly lower values (i.e., ~19% for the average slip and ~25% for the average recurrence time), the parameters derived from the 2-min fall within the variability of parameters from the 15-min models (Figure S15 in Supporting Information S1), testifying that the short observation time is enough to capture the model behavior and the similarity between different models.

5. Conclusions

We developed *Foamquake*, a novel analog setup simulating the seismic cycle of subduction megathrusts. The elastoplastic model experiences quasi-periodic cycles of stress accumulation and sudden release through spontaneous nucleation of frictional instabilities, called foamquakes. The representativeness of modeling results has been assessed by investigating repeatability and completeness of the experimental recurrence histories. Through a systematic analysis of model sensitivity to the seismogenic zone length and to the normal load, we identified the best scaled single-asperity model configuration with respect to the natural prototype. This model generates slip phases properly scaled in terms of coseismic displacement amplitude. Additionally, the generated analog earthquakes share similar source parameters scaling as natural interplate earthquakes.

Models with two asperities divided by a barrier highlight the importance of the 3D nature of the subduction megathrust to take into account the observed complexity of rupture patterns in space and time. The coexistence of full and partial ruptures with different R_T, long-term complementary rupture sequences, rupture cascades and superimposed cycles, demonstrates that *Foamquake* reproduces the space-time rupture behavior of natural subduction zones. Together with barriers, physical properties of asperities control seismic behavior. This is particularly interesting when asperities properties are dissimilar. Asperities synchronization (which may lead to the origin of mega-earthquakes) is observed preferentially for asperities with similar properties and low yield strength. Experimental results suggest that long earthquake histories are needed to properly evaluate the earthquake recurrence variability of subduction megathrusts. Experimental results can be compared with numerical models based on the rate and state framework to make quantitative comparisons to asperities interaction theory.

This study confirms the importance of analog modeling as a useful tool to overcome the paucity of direct observations from the natural prototype. Our model can afford new insights into how the megathrust frictional segmentation controls the long-term recurrence of interplate earthquakes. *Foamquake* can be further tuned to perform parametric studies on other megathrust properties, for mimicking specific frictional configurations from real subduction zones and to draw new inferences about the underlying physical processes governing the stick-slip behavior, investigating the nucleation and propagation of frictional instabilities within the granular shear zone.

Data Availability Statement

Material properties data are available open access in Mastella, Corbi, Funiciello, Rosenau et al. (2021) http://doi.org/10.5880/fidgeo.2021.047). PIV Data and codes underlying this study are published open access in Mastella, Corbi, Funiciello and Matthias et al. (2021, http://doi.org/10.5880/fidgeo.2021.046).

Acknowledgments

This study has been financially supported by the EPOS Research Infrastructure through the contribution of the Italian Ministry of University and Research (MUR)- EPOS ITALIA Joint Research Unit. The Grant to the Department of Science, Roma Tre University (MIUR-Italy Dipartimenti di Eccellenza, ARTICOLO 1, COMMI 314 – 337 LEGGE 232/2016) is gratefully acknowledged. Matthias Rosenau has been supported by Deutsche Forschungsgemeinschaft (DFG) through grant CRC 1114 "Scaling Cascades in Complex Systems", Project Number 235221301, Project B01. The authors also thank the reviewers Y. Caniven, P. Ampuero, and I. Manighetti for constructive comments. Michael Rudolf and Ehsan Kosari are acknowledged for their contribution in characterizing the analogue materials used in *Foamquake* (Mastella, Corbi, Funiciello, Rosenau et al., 2021, GFZ Data Services). The authors thank GFZ Data Services for publishing the data. Monica Moroni is acknowledged for the invaluable help with monitoring systems. In Figures 2 and 5 we used the perceptually uniform color maps *Lajolla* and *Oslo* and in Figure 4 the colormap Imola devised by F. Crameri.

References

Ando, M. (1975). Source mechanisms and tectonic significance of historical earthquakes along the Nankai Trough. *Tectonophysics*, *27*, 119–140. https://doi.org/10.1016/0040-1951(75)90102-X

Anooshehpoor, A., & Brune, J. N. (1994). Frictional heat generation and seismic radiation in a foam rubber model of earthquakes. *Pure and Applied Geophysics*, *142*, 735–747. https://doi.org/10.1007/bf00876062

Anooshehpoor, A., & Brune, J. N. (1999). Wrinkle-like weertman pulse at the interface between two blocks of foam rubber with different velocities. *Geophysical Research Letters*, *26*(13), 2025–2028. https://doi.org/10.1029/1999gl900397

Archuleta, R. J., & Brune, J. N. (1975). Surface strong motion associated with a stick-slip event in a foam rubber model of earthquakes. *Bulletin of the Seismological Society of America*, *65*, 1059–1071. https://doi.org/10.1785/bssa0650051059

Atwater, B. F., & Griggs, G. B. (2012). *Deep-sea turbidites as guides to holocene earthquake history at the Cascadia subduction zoned alternative views for a seismic-hazard workshop*. U.S. Geological Survey. Open-File Report, 2012e1043.

Barbot. (2019). Slow-slip, slow earthquakes, period-two cycles, full and partial ruptures, and deterministic chaos in a single asperity fault. *Tectonophysics*, 768. https://doi.org/10.1016/j.tecto.2019.228171

Beck, S., Barrientos, S., Kausel, E., & Reyes, M. (1998). Source characteristics of historic earthquakes along the central Chile subduction zone. *Journal of South American Earth Sciences*, *11*, 115–129. https://doi.org/10.1016/S0895-9811(98)00005-4

Ben-Zion, Y., & Rice, J. R. (1993). Earthquake failure sequences along a cellular fault zone in a three-dimensional elastic solid containing asperity and nonasperity regions. *Journal of Geophysical Research*, *98*, 14109–14131. https://doi.org/10.1029/93JB01096

Bilek, S. (2007). Influence of subducting topography on earthquake rupture. In T. H. Dixon, & J. Casey Moore (Eds.), *The seismogenic zone of subduction thrust faults* (pp. 123–146). New York: Columbia University Press. https://doi.org/10.7312/dixo13866-005

Blaser, L., Krüger, F., Ohrnberger, M., & Scherbaum, F. (2010). Scaling relations of earthquake source parameter estimates with special focus on subduction environment. *Bulletin of the Seismological Society of America*, *100*(6), 2914–2926. https://doi.org/10.1785/0120100111

Bletery, Q., Sladen, A., Delouis, B., Vallée, M., Nocquet, J.-M., Rolland, L., & Jiang, J. (2014). A detailed source model for the Mw9.0 Tohoku-Oki earthquake reconciling geodesy, seismology, and tsunami records. *Journal of Geophysical Research: Solid Earth*, *119*, 7636–7653. https://doi.org/10.1002/2014JB011261

Bookhagen, B., Echtler, H. P., Melnick, D., Strecker, M. R., & Spencer, J. Q. G. (2006). Using uplifted Holocene beach berms for paleoseismic analysis on the Santa Maria Island, south-central Chile. *Geophysical Research Letters*, *33*, L15302. https://doi.org/10.1029/2006GL026734

Brizzi, S., Sandri, L., Funiciello, F., Corbi, F., Piromallo, C., & Heuret, A. (2018). Multivariate statistical analysis to investigate the subduction zone parameters favoring the occurrence of giant megathrust earthquakes. *Tectonophysics*, *728–729*, 92–103. https://doi.org/10.1016/j.tecto.2018.01.027

Brizzi, S., Zelst, I., Funiciello, F., Corbi, F., & Dinther, Y. (2020). How sediment thickness influences subduction dynamics and seismicity. *Journal of Geophysical Research: Solid Earth*, *125*, e2019JB018964. https://doi.org/10.1029/2019jb018964

Brune, J. N. (1973). Earthquake modeling by stick-slip along precut surfaces in stressed foam rubber. *Bulletin of the Seismological Society of America*, *63*, 2105–2119. https://doi.org/10.1785/bssa0636-12105

Brune, J. N. (1996). Particle motion in a physical model of shallow angle thrust faulting. *Proceedings of the Indian Academy of Sciences — Section A*, *105*, 197–206. https://doi.org/10.1007/bf02876014

Brune, J. N., & Anooshehpoor, A. (1997). Frictional resistance of a fault zone with strong rotors. *Geophysical Research Letters*, *24*, 2071–2074. https://doi.org/10.1029/97gl01941

Brune, J. N., Brown, S., & Johnson, P. A. (1993). Rupture mechanism and interface separation in foam rubber models of earthquakes: A possible solution to the heat flow paradox and the paradox of large overthrusts. *Tectonophysics*, 59–67.

Brune, J. N., Johnson, P. A., & Slater, C. (1990). Nucleation, predictability, and rupture mechanism in foam rubber models of earthquakes. *Journal of Himalayan Geology*, *1*, 155–166.

Caniven, Y., & Dominguez, S. (2021). Validation of a multilayered analog model integrating crust-mantle visco-elastic coupling to investigate subduction megathrust earthquake cycle. *Journal of Geophysical Research: Solid Earth*, *126*, e2020JB020342. https://doi.org/10.1029/2020JB020342

Caniven, Y., Dominguez, S., Soliva, R., Cattin, R., Peyret, M., Marchandon, M., et al. (2015). A new multilayered visco-elasto-plastic experimental model to study strike-slip fault seismic cycle. *Tectonics*, *34*, 232–264. https://doi.org/10.1002/2014TC003701

Caniven, Y., Dominguez, S., Soliva, R., Peyret, M., Cattin, R., & Maerten, F. (2017). Relationships between along-fault heterogeneous normal stress and fault slip patterns during the seismic cycle: Insights from a strike-slip fault laboratory model Earth Planet. *Science Letter*, *480*, 147–157. https://doi.org/10.1016/j.epsl.2017.10.009

Carvajal, M., Cisternas, M., Gubler, A., Catalan, P. A., Winckler, P., & Wesson, R. L. (2017). Reexamination of the magnitudes for the 1906 and 1922 Chilean earthquakes using Japanese tsunami amplitudes: Implications for source depth constraints. *Journal of Geophysical Research: Solid Earth*, *122*, 4–17. https://doi.org/10.1002/2016JB013269

Cochard, A., & Madariaga, R. (1996). Complexity of seismicity due to highly rate-dependent friction. *Journal of Geophysical Research*, *101*, 25321–25336. https://doi.org/10.1029/96JB02095

Contreras-Reyes, E., & Carrizo, D. (2011). Control of high oceanic features and subduction channel on earthquake ruptures along the Chile-Peru subduction zone. *Physics of the Earth and Planetary Interiors*, *186*(1–2), 49–58. https://doi.org/10.1016/j.pepi.2011.03.002

Corbi, F., Bedford, J., Sandri, L., Funiciello, F., Gualandi, A., & Rosenau, M. (2020). Predicting imminence of analog megathrust earthquakes with machine learning: Implications for monitoring subduction zones. *Geophysical Research Letters*, *47*, e2019GL086615. https://doi.org/10.1029/2019GL086615

Corbi, F., Funiciello, F., Brizzi, S., Lallemand, S., & Rosenau, M. (2017). Control of asperities size and spacing on seismic behavior of subduction megathrusts. *Geophysical Research Letters*, *44*, 8227–8235. https://doi.org/10.1002/2017GL074182

Corbi, F., Funiciello, F., Faccenna, C., Ranalli, G., & Heuret, A. (2011). Seismic variability of subduction thrust faults: Insights from laboratory models. *Journal of Geophysical Research*, *116*, B06304. https://doi.org/10.1029/2010jb007993

Corbi, F., Funiciello, F., Moroni, M., Van Dinther, Y., Mai, P. M., Dalguer, L. A., & Faccenna, C. (2013). The seismic cycle at subduction thrusts: 1. Insights from laboratory models. *Journal of Geophysical Research: Solid Earth*, *118*, 1483–1501. https://doi.org/10.1029/2012JB009481

Corbi, F., Herrendörfer, R., Funiciello, F., & Dinthervan, Y. (2017). Controls of seismogenic zone width and subduction velocity on interplate seismicity: Insights from analog and numerical models. *Geophysical Research Letters*, *44*, 6082–6091. https://doi.org/10.1002/2016GL072415

Corbi, F., Sandri, L., Bedford, J., Funiciello, F., Brizzi, S., Rosenau, M., & Lallemand, S. (2019). Machine learning can predict the timing and size of analog earthquakes. *Geophysical Research Letters*, *46*(3), 1303–1311. https://doi.org/10.1029/2018GL081251

Dal Zilio, L., Lapusta, N., & Avouac, J. P. (2020). Unraveling scaling properties of slow-slip events. *Geophysical Research Letters*, *47*, e2020GL087477. https://doi.org/10.1029/2020GL087477

den Hartog, S. A. M., Niemeijer, A. R., & Spiers, C. J. (2012). New constraints on megathrust slip stability under subduction zone P–T conditions. *Earth and Planetary Science Letters*, *353*, 240–252. https://doi.org/10.1016/j.epsl.2012.08.022

Dieterich, J. H., & Linker, M. F. (1992). Fault stability under conditions of variable normal stress. *Geophysical Research Letters*, *19*, 1691–1694. https://doi.org/10.1029/92gl01821

Dominguez, S., Malavieille, J., Mazzotti, S., Martin, N., Caniven, Y., Cattin, R., et al. (2015). Modeling subduction megathrust earthquakes: Insights from a viscoelasto-plastic analog model. *Geophysical Research Abstracts*, *17*, EGU2015–15200.

Dublanchet, P. (2019). Scaling and variability of interacting repeating earthquake sequences controlled by asperity density. *Geophysical Research Letters*, *46*, 11950, 11958, https://doi.org/10.1029/2019GL084614

Dublanchet, P., Bernard, P., & Favreau, P. (2013). Interactions and triggering in a 3-D rate-and-state asperity model. *Journal of Geophysical Research: Solid Earth*, *118*, 2225–2245. https://doi.org/10.1002/jgrb.50187

Ester, M., Kriegel, H.-P., Sander, J., & Xu, X. (1996) A density-based algorithm for discovering clusters in large spatial databases with noise In *Proceedings of the second international conference on knowledge discovery and data mining* (Vol. 96, pp. 226–231). Portland, OR: AAAI Press.

Fujiwara, O., Aoshima, A., Irizuki, T., Ono, E., Obrochta, S. P., Sampei, Y., et al. (2020). Tsunami deposits refine great earthquake rupture extent and recurrence over the past 1300 years along the Nankai and Tokai fault segments of the Nankai Trough, Japan. *Quaternary Science Reviews*, *227*, 105999. https://doi.org/10.1016/j.quascirev.2019.105999

Garrett, E., Fujiwara, O., Riedesel, S., Walstra, J., Deforce, K., Yokoyama, Y., et al. (2018). Historical Nankai-Suruga megathrust earthquakes recorded by tsunami and terrestrial mass movement deposits on the Shirasuka coastal lowlands, Shizuoka Prefecture, Japan. *The Holocene*, *28*, 968, 983. https://doi.org/10.1177/0959683617752844

Goes, S. D. B., (1996). Irregular recurrence of large earthquakes: An analysis of historic and paleoseismic catalogs. *Journal of Geophysical Research*, *101* (B3), 5739–5749. https://doi.org/10.1029/95JB03044

Goldfinger, C., Nelson, C. H., Morey, A., Johnson, J. E., Gutierrez-Pastor, J., Eriksson, A. T., et al. (2012). Turbidite event history-methods and implications for Holocene paleoseismicity of the Cascadia subduction zone. USGS Professional Paper 1661-F (pp. 184). Reston, VA: U.S. Geological Survey. https://doi.org/10.3133/pp1661F

Gomberg, J., Wech, A., Creager, K., Obara, K., & Agnew, D. (2016). Reconsidering earthquake scaling. *Geophysical Research Letters*, *43*, 6243–6251. https://doi.org/10.1002/2016GL069967

Hanks, T. C., & Kanamori, H. (1979). A moment magnitude scale. *Journal of Geophysical Research*, *84*(5), 2348–2350. https://doi.org/10.1029/JB084iB05p02348

Hasegawa, A., Yoshida, K., & Okada, T. (2011). Nearly complete stress drop in the 2011 Mw 9.0 off the Pacific coast of Tohoku earthquake. *Earth Planets and Space*, *63*, 703–707. https://doi.org/10.5047/eps.2011.06.007

Heuret, A., Conrad, C., Funiciello, F., Lallemand, S., & Sandri, L. (2012). Relation between subduction megathrust earthquakes, trench sediment thickness and upper plate strain. *Geophysical Research Letters*, *39*, 05304. https://doi.org/10.1029/2011GL050712

Heuret, A., Lallemand, S., Funiciello, F., Piromallo, C., & Faccenna, C. (2011). Physical characteristics of subduction interface type seismogenic zones revisited. *Geochemistry, Geophysics, Geosystems*, *12*, Q01004. https://doi.org/10.1029/2010GC003230

Houston, H. (2001). Influence of depth, focal mechanism, and tectonic setting on the shape and duration of earthquake source time functions. *Journal of Geophysical Research*, *106*, 11137–11150. https://doi.org/10.1029/2000JB900468

Hubbert, M. K. (1937). Theory of scale models as applied to the study of geological structures. *The Geological Society of America Bulletin*, *48*, 1459–1520. https://doi.org/10.1130/gsab-48-1459

Hyndman, R. D., Yamano, M., & Oleskevich, D. A. (1997). The seismogenic zone of subduction thrust faults. *Island Arc*, *6*, 244–260. https://doi.org/10.1111/j.1440-1738.1997.tb00175.x

Ide, S., Beroza, G. C., Shelly, D. R., & Uchide, T. (2007). A scaling law for slow earthquakes. *Nature*, *447*, 76–79. https://doi.org/10.1038/nature05780

Ide, S., Imanishi, K., Yoshida, Y., Beroza, G. C., & Shelly, D. R. (2008). Bridging the gap between seismically and geodetically detected slow earthquakes. *Geophysical Research Letters*, *35*, L10305. https://doi.org/10.1029/2008GL034014

Kanamori, H., & Anderson, L. (1975). Theoretical basis of some empirical relations in seismology. *Bulletin of the Seismological Society of America*, *65*, 1073–1095.

Kaneko, Y., Avouac, J.-P., & Lapusta, N. (2010). Towards inferring earthquake patterns from geodetic observations of interseismic coupling. *Nature Geoscience*, *3*(5), 363–369. https://doi.org/10.1038/ngeo843

Kato, N. (2014). Deterministic chaos in a simulated sequence of slip events on a single isolated asperity. *Geophysical Journal International*, *198* (2), 727–736. https://doi.org/10.1093/gji/ggu157

Kitamura, A., Seki, Y., Kitamura, Y., & Haga, T. (2018). The discovery of emerged boring bivalves at cape Omaezaki, Shizuoka, Japan: Evidence for the 1361 CE Tokai earthquake along the Nankai trough. *Marine Geology*, *405*, 114–119. https://doi.org/10.1016/j.margeo.2018.08.006

Kodaira, S., Hori, T., Ito, A., Miura, S., Fujie, G., Park, J.-O., et al. (2006). A cause of rupture segmentation and synchronization in the Nankai Trough revealed by seismic imaging and numerical simulation. *Journal of Geophysical Research*, *111*. https://doi.org/10.1029/2005JB004030

Konca, A. O., Avouac, J.-P., Sladen, A., Meltzner, A. J., Sieh, K., Fang, P., et al. (2008). Partial rupture of a locked patch of the Sumatra megathrust during the 2007 earthquake sequence. *Nature*, *456*(7222), 631–635. https://doi.org/10.1038/nature07572

Kosari, E., Rosenau, M., Bedford, J., Rudolf, M., & Oncken, O. (2020). On the relationship between offshore geodetic coverage and slip model uncertainty: Analog megathrust earthquake case studies. *Geophysical Research Letters*, *47*(15), e2020GL088266. https://doi.org/10.1029/2020gl088266

Kuehn, N. M., Hainzl, S., & Scherbaum, F. (2008). Non-Poissonian earthquake occurrence in coupled stress release models and its effect on seismic hazard. *Geophysical Journal International*, *174*, 649–658. https://doi.org/10.1111/j.1365-246X.2008.03835.x

Kulkarni, R., Wong, I., Zachariasen, J., Goldfinger, C., & Lawrence, M. (2013). Statistical analyses of great earthquake recurrence along the Cascadia subduction zone. *Bulletin of the Seismological Society of America*, *103*, 3205, 3221. https://doi.org/10.1785/0120120105

Lajoie, K. R. (1986). Coastal tectonics. In *Active tectonics, studies in geophysics* (pp. 95–124). Washington, D. C: National Academic Press.

Lay, T., & Kanamori, H. (1981). An asperity model of large earthquake sequences. *Earthquake Prediction*, *4*, 579–592.

Lay, T., Kanamori, H., Ammon, C. J., Koper, K. D., Hutko, A. R., Ye, L., et al. (2012). Depth-varying rupture properties of subduction zone megathrust faults. *Journal of Geophysical Research*, *117*(B4), B04311. https://doi.org/10.1029/2011JB009133

Lay, T., Kanamori, H., & Ruff, L. J. (1982). The asperity model and the nature of large subduction zone earthquakes. *Earthquake Prediction Research*, *1982*(1), 3–71.

Lilliefors, H. W. (1969). On the Kolmogorov-Smirnov test for the exponential distribution with mean unknown. *Journal of the American Statistical Association*, *64*(325), 387–389. https://doi.org/10.1080/01621459.1969.10500983

Lui, S. K., & Lapusta, N. (2018). Modeling high stress drops, scaling, interaction, and irregularity of repeating earthquake sequences near Parkfield. *Journal of Geophysical Research: Solid Earth*, *123*, 10854–10879. https://doi.org/10.1029/2018JB016472

Luttrell, K., Tong, X., Sandwell, D., Brooks, B., & Bevis, M. (2011). Estimates of stress drop and crustal tectonic stress from the 27 February 2010 Maule Chile, earthquake: Implications for fault strength. *Journal of Geophysical Research*, *116*, B11401. https://doi.org/10.1029/2011JB008509

Ma, S., & He, C. (2001). Period doubling as a result of slip complexities in sliding surfaces with strength heterogeneity, *Tectonophysics*, *337*, 135–145. https://doi.org/10.1016/S0040-1951(01)00114-7

Mastella, G., Corbi, F., Funiciello, F., & Matthias, R. (2021). *Particle image correlation data from foamquake: A novel seismotectonic analog model mimicking the megathrust seismic cycle*. GFZ Data Services. https://doi.org/10.5880/fidgeo.2021.046

Mastella, G., Corbi, F., Funiciello, F., Rosenau, M., Rudolf, M., & Kosari, E. (2021). *Properties of rock analogue materials used for foamquake: A novel seismotectonic analog model mimicking the megathrust seismic cycle at RomaTre university (Italy)*. GFZ data Services. https://doi.org/10.5880/fidgeo.2021.047

McCalpin, J. P. (2009). Chapter 9: Application of paleoseismic data to seismic hazard assessment and neotectonic research. In McCalpin, J. P. (Ed.), *Paleoseismology* (2nd ed.,). *International geophysics series* (Vol. 95, pp. 1–106). Elsevier Publishing, https://doi.org/10.1016/S0074-6142(09)95009-4

Mele Veedu, D., Giorgetti, C., Scuderi, M., Barbot, S., Marone, C., & Collettini, C. (2020). Bifurcations at the stability transition of earthquake faulting. *Geophysical Research Letters*, *47*, e2020GL087985. https://doi.org/10.1029/2020GL087985

Mele Veedu, M., & Barbot, S. (2016). The parkfield tremors reveal slow and fast ruptures on the same asperity. *Nature*, *532* (7599), 361–365. https://doi.org/10.1038/nature17190

Melnick, D., Bookhagen, B., Strecker, M. R., & Echtler, H. P. (2009). Segmentation of megathrust rupture zones from fore-arc deformation patterns over hundreds to millions of years, Arauco peninsula, Chile. *Journal of Geophysical Research*, *114*. https://doi.org/10.1029/2008JB005788

Melnick, D., Moreno, M., Quinteros, J., Baez, J. C., Deng, Z., Li, S., & Oncken, O. (2017). The super-interseismic phase of the megathrust earthquake cycle in Chile. *Geophysical Research Letters*, *44*, 784–791. https://doi.org/10.1002/2016GL071845

Michel, S., Gualandi, A., & Avouac, J. P. (2019). Similar scaling laws for earthquakes and Cascadia slow-slip events. *Nature*, *574*, 522–526. https://doi.org/10.1038/s41586-019-1673-6

Moernaut, J. (2020). Time-dependent recurrence of strong earthquake shaking near plate boundaries: A lake sediment perspective. *Earth-Science Reviews*, *210*, 103344. https://doi.org/10.1016/j.earscirev.2020.103344

Moernaut, J., Van Daele, M., Heirman, K., Fontijn, K., Strasser, M., Pino, M., et al. (2014). Lacustrine turbidites as a tool for quantitative earthquake reconstruction: New evidence for a variable rupture mode in south central Chile. *Journal of Geophysical Research: Solid Earth*, *119*, 1607–1633. https://doi.org/10.1002/2013JB010738

Moreno, M., Bolte, J., Klotz, J., & Melnick, D. (2009). Impact of megathrust geometry on inversion of coseismic slip from geodetic data: Application to the 1960 Chile earthquake. *Geophysical Research Letters*, *36*, L16310. https://doi.org/10.1029/2009GL039276

Murotani, S., Miyake, H., & Koketsu, K. (2008). Scaling of characterized slip models for plate-boundary earthquakes. *Earth Planets and Space*, *60*, 987–991. https://doi.org/10.1186/BF03352855

Murotani, S., Satake, K., & Fujii, Y. (2013). Scaling relations of seismic moment, rupture area, average slip, and asperity size for M ∼ 9 subduction-zone earthquakes. *Geophysical Research Letters*, *40*(19), 5070–5074. https://doi.org/10.1002/grl.50976

Natawidjaja, D. H., Sieh, K., Chlieh, M., Galetzka, J., Suwargadi, B. W., Cheng, H., et al. (2006). Source parameters of the great Sumatran megathrust earthquakes of 1797 and 1833 inferred from coral microatolls. *Journal of Geophysical Research*, *111*, B06403. https://doi.org/10.1029/2005JB004025

Natawidjaja, D. H., Sieh, K., Ward, S. N., Cheng, H., Edwards, R. L., Galetzka, J., & Suwargadi, B. W. (2004). Paleogeodetic records of seismic and aseismic subduction from central Sumatran microatolls, Indonesia. *Journal of Geophysical Research*, *109*(B4), 1–34. https://doi.org/10.1029/2003JB002398

Nocquet, JM., Jarrin, P., Vallée, M., Mothes, P. A., Grandin, R., Rolandone, F., et al. (2017). Supercycle at the Ecuadorian subduction zone revealed after the 2016 Pedernales earthquake. *Nature Geoscience*, *10*, 145–149. https://doi.org/10.1038/ngeo2864

Noda, A., TuZino, T., Kanai, Y., Furukawa, R., & Uchida, J. (2008). Paleoseismicity along the southern Kuril Trench deduced from submarine-fan turbidites. *Marine Geology*, *254*, 73–90. https://doi.org/10.1016/j.margeo.2008.05.015

Okubo, P. G., & Dieterich, J. H. (1984). Effects of physical fault properties on frictional instabilities produced on simulated faults. *Journal of Geophysical Research*, *89*, 5817–5827. https://doi.org/10.1029/JB089iB07p05817

Pacheco, J. F., & Sykes, L. R. (1992). Seismic moment catalog of large shallow earthquakes, 1900 to 1989. *Bulletin of the Seismological Society of America*, *82*, 13062–1349. TDFMEE. https://doi.org/10.1785/bssa0820031306

Peng, Z., & Gomberg, J. (2010). An integrated perspective of the continuum between earthquakes and slow-slip phenomena. *Nature Geoscience*, *3*, 599–607. https://doi.org/10.1038/ngeo940

Philibosian, B., & Meltzner, A. J. (2020). *Segmentation and supercycles: A catalog of earthquake rupture patterns from the Sumatran Sunda megathrust and other well-studied faults worldwide*. https://doi.org/10.1016/j.quascirev.2020.106390

Rabinowitz, H. S., Savage, H. M., Skarbek, R. M., Ikari, M. J., Carpenter, B. M., & Collettini, C. (2018). Frictional behavior of input sediments to the Hikurangi Trench, New Zealand. *Geochemistry, Geophysics, Geosystems*, *19*, 2973–2990. https://doi.org/10.1029/2018GC007633

Rosakis, A. J., Xia, K., Lykotrafitis, G., & Kanamori, H. (2007). In G. Schubert (Ed.), *4.08 – Dynamic shear rupture in frictional interfaces: Speeds, directionality, and modes A2* (Vol. 83–213). Oxford: Elsevier.

Rosenau, M., Corbi, F., & Dominguez, S. (2017). Analogue earthquakes and seismic cycles: Experimental modelling across timescales. *Solid Earth*, *8*, 1–635. https://doi.org/10.5194/se-8-597-2017

Rosenau, M., Horenko, I., Corbi, F., Rudolf, M., Kornhuber, R., & Oncken, O. (2019). Synchronization of great subduction megathrust earthquakes: Insights from scale model analysis. *Journal of Geophysical Research: Solid Earth*, *124*(4), 3646–3661. https://doi.org/10.1029/2018JB016597

Rosenau, M., Lohrmann, J., & Oncken, O. (2009). Shocks in a box: An analogue model of subduction earthquake cycles with application to seismotectonic forearc evolution. *Journal of Geophysical Research*, *114*(B1), 1–20. https://doi.org/10.1029/2008JB005665

Rosenau, M., Nerlich, R., Brune, S., & Oncken, O. (2010). Experimental insights into the scaling and variability of local tsunamis triggered by giant subduction megathrust earthquakes. *Journal of Geophysical Research*, *115*, B09314. https://doi.org/10.1029/2009JB007100

Rosenau, M., & Oncken, O. (2009). Fore-arc deformation controls frequency-size distribution of megathrust earthquakes in subduction zones. *Journal of Geophysical Research*, *114*, B10311. https://doi.org/10.1029/2009JB006359

Ruff, L. J. (1996). Large earthquakes in subduction zones: Segment interaction and recurrence times. In G. E. Bebout, D. W. Scholl, S. H. Kirby, & J. P. Platt (Eds.), *Subduction top to bottom 338* (pp. 91–104). Washington, DC: American Geophysical Union.

Salditch, L., Stein, S., Neely, J., Spencer, B. D., Brooks, E. M., Agnon, A., & Liu, M. (2020). Earthquake supercycles and long-term fault memory. *Tectonophysics*, *774*, 228–289. https://doi.org/10.1016/j.tecto.2019.228289

Satake, K. (2015). Geological and historical evidence of irregular recurrent earthquakes in Japan. *Philosophical Transactions of the Royal Society A: Mathematical, Physical & Engineering Sciences*, *373*, 20140375. https://doi.org/10.1098/rsta.2014.0375

Satake, K., & Atwater, B. F. (2007). Long-term perspectives on giant earthquakes and tsunamis at subduction zones. *Annual Review of Earth and Planetary Sciences*, *35*, 349–374. https://doi.org/10.1146/annurev.earth.35.031306.140302

Satake, K., Fujii, Y., Harada, T., & Namegaya, Y. (2013). Time and space distribution of coseismic slip of the 2011 Tohoku earthquake as inferred from tsunami waveform data. *Bulletin of the Seismological Society of America*, *103* (2B), 1473–1492. https://doi.org/10.1785/0120120122

Schäfer, A. M., & Wenzel, F. (2019). Global megathrust earthquake hazard—Maximum magnitude assessment using multi-variate machine learning. *Frontiers of Earth Science*, *7*(June), 1–19. https://doi.org/10.3389/feart.2019.00136

Schellart, W. P., & Rawlinson, N. (2013). Global correlations between maximum magnitudes of subduction zone interface thrust earthquakes and physical parameters of subduction zones. *Physics of the Earth and Planetary Interiors*, *225*, 41–67. https://doi.org/10.1016/j.pepi.2013.10.001

Scholz, C. H. (1990). Earthquakes as chaos. *Nature*, *348*, 197–198. https://doi.org/10.1038/348197a0

Scholz, C. H., Molnar, P., & Johnson, T. (1972). Detailed studies of frictional sliding of granite and implications for the earthquake mechanism. *Journal of Geophysical Research*, *77*, 6392–6406. https://doi.org/10.1029/JB077i032p06392

Scholz, C. H., & Small, C. (1997). The effect of seamount subduction on seismic coupling. *Geology*, *25*, 487–490. https://doi.org/10.1130/0091-7613(1997)025<0487:teosso>2.3.co;2

Scuderi, M., Marone, C., Tinti, E., Di Stefano, G., Collettini, C. (2016). Precursory changes in seismic velocity for the spectrum of earthquake failure modes. *Nature Geoscience*, *9*, 695–700. https://doi.org/10.1038/ngeo2775

Shelly, D. R. (2010). Periodic, chaotic, and doubled earthquake recurrence intervals on the Deep San Andreas fault. *Science*, *328*, 1385–1388. https://doi.org/10.1126/science.1189741

Smardzewski, J., Grbac, I., & Prekrat, S. (2008). Nonlinear mechanics of hyper elastic polyurethane furniture foams. *Drvna Industrija*, *59*(1), 23–28.

Sobolev, S. V., & Muldashev, I. A. (2017). Modeling seismic cycles of great megathrust earthquakes across the scales with focus at postseismic phase. *Geochemical Geophysical Geosystem*, *18*, 4387–4408. https://doi.org/10.1002/2017GC007230

Stein, S., & Newman, A. V. (2004). Characteristic and uncharacteristic earthquakes as possible artifacts: What does the seismic history actually tell us? *Seismological Research Letters*, *75*(5), 613. https://doi.org/10.1785/gssrl.75.5.613

Strasser, F. O., Arango, M. C., & Bommer, J. J. (2010). Scaling of the source dimensions of interface and intraslab subduction-zone earthquakes with moment magnitude. *Seismological Research Letters*, *81*, 951–950. https://doi.org/10.1785/gssrl.81.6.941

Subarya, C., Chlieh, M., Prawirodirdjo, L., Avouac, J. P., Bock, Y., Sieh, K., et al. (2006). Plate-boundary deformation associated with the great Sumatra-Andaman earthquake. *Nature*, *440*(7080), 46–51. https://doi.org/10.1038/nature04522

Sveen, J. K. (2004). *An introduction to matpiv v.1.6.1 Eprint no. 2*. Department of Mathematics, University of Oslo. ISSN 0809-4403. Retrieved from http://www.math.uio.no/$jks/matpiv

Tsuda, K., Iwase, S., Uratani, H., Ogawa, S., Watanabe, T., Miyakoshi, J., & Ampuero, J. P. (2017). Dynamic rupture simulations based on the characterized source model of the Tohoku earthquake. *PAGE*, *174*, 3357–3368. https://doi.org/10.1007/s00024-016-1446-1

Turcotte, D., & Schubert, G. (2014). *Geodynamics* (3rd ed.,). Cambridge University Press.

van Dinther, Y., Gerya, T. V., Corbi, F., Dalguer, L. A., Funiciello, F., & Mai, P. M. (2013). The seismic cycle at subduction thrusts: 2. Benchmarking geodynamic numerical simulations and analogue models. *Journal of Geophysical Research*. https://doi.org/10.1002/jgrb.20048

van Rijsingen, E., Lallemand, S., Peyret, M., Arcay, D., Heuret, A., Funiciello, F., & Corbi, F. (2018). How subduction interface roughness influences the occurrence of large interplate earthquakes. *Geochemistry, Geophysics, Geosystems*, *19*(8), 2342–2370. https://doi.org/10.1029/2018GC007618

Wang, W., & Scholz, C. H. (1994). Micromechanics of the velocity and normal stress dependence of rock friction. *PAGE*, *143*, 303–315. https://doi.org/10.1007/BF00874333

Yue, H., Lay, T., Rivera, L., An, C., Vigny, C., Tong, X., & Báez Soto, J. C. (2014). Localized fault slip to the trench in the 2010 Maule, Chile Mw = 8.8 earthquake from joint inversion of high-rate GPS, teleseismic body waves, InSAR, campaign GPS, and tsunami observations. *Journal of Geophysical Research: Solid Earth*, *119*, 7786–7804. https://doi.org/10.1002/2014JB011340